

## ACCEPTED VERSION

Okin, Gregory S.; Clarke, Kenneth David; Lewis, Megan Mary  
[Comparison of methods for estimation of absolute vegetation and soil fractional cover using MODIS normalized BRDF-adjusted reflectance data](#), Remote Sensing of Environment, 2013; 130:266-279.

Copyright © 2012 Elsevier Inc. All rights reserved.

### PERMISSIONS

<http://www.elsevier.com/wps/find/authorsview.authors/postingpolicy>

Policy: Authors retain the right to use the accepted author manuscript for personal use, internal institutional use and for permitted scholarly posting provided that these are not for purposes of **commercial use** or **systematic distribution**.

Elsevier believes that individual authors should be able to distribute their AAMs for their personal voluntary needs and interests, e.g. posting to their websites or their institution's repository, e-mailing to colleagues.

15<sup>th</sup> January, 2013

<http://hdl.handle.net/2440/74875>

1     **Comparison of methods for estimation of absolute vegetation and soil fractional cover**  
2             **using MODIS Normalized BRDF-Adjusted Reflectance Data**

3

4     Gregory S. Okin<sup>1,†</sup>, Kenneth D. Clarke<sup>2</sup>, Megan M. Lewis<sup>2</sup>

5     <sup>1</sup> Department of Geography, University of California, Los Angeles, CA 90095

6     <sup>2</sup> School of Earth and Environmental Sciences, The University of Adelaide, Adelaide,  
7     Australia, 5005

8

9     <sup>†</sup> Corresponding Author. Email: okin@ucla.edu

10

11     **Abstract**

12     Green vegetation (GV), nonphotosynthetic vegetation (NPV), and soil are important  
13     ground cover components in terrestrial ecosystems worldwide. There are many good  
14     methods for observing the dynamics of GV with optical remote sensing, but there are  
15     fewer good methods for observing the dynamics of NPV and soil. Given the difficulty of  
16     remotely deriving information on NPV and soil, the purpose of this study is to evaluate  
17     several methods for the retrieval of information on fractional cover of GV, NPV, and  
18     soil using 500-m MODIS nadir BRDF-adjusted reflectance (NBAR) data. In particular,  
19     three spectral mixture analysis (SMA) techniques are evaluated: simple SMA, multiple-  
20     endmember SMA (MESMA), and relative SMA (RSMA). *In situ* cover data from  
21     agricultural fields in Southern Australia are used as the basis for comparison. RSMA  
22     provides an index of fractional cover of GV, NPV, and soil, so a method for converting  
23     these to absolute fractional cover estimates is also described and evaluated. All  
24     methods displayed statistically significant correlations with *in situ* data. All methods  
25     proved equally capable at predicting the dynamics of GV. MESMA predicted NPV  
26     dynamics best. RSMA predicted dynamics of soil best. The method for converting RSMA

27 indices to fractional cover estimates provided estimates that were comparable to those  
28 provided by SMA and MESMA. Although it does not always provide the best estimates  
29 of ground component dynamics, this study shows that RSMA indices are useful  
30 indicators of GV, NPV, and soil cover. However, our results indicate that the choice of  
31 unmixing technique and its implementation ought to be application-specific, with  
32 particular emphasis on which ground cover retrieval requires the greatest accuracy  
33 and how much ancillary data is available to support the analysis.

34 **Keywords**

35 Remote sensing, MODIS, vegetation indices, nonphotosynthetic vegetation, fractional  
36 cover, soil, field spectroscopy, validation

37

## 38 **Introduction**

39 Vegetation dynamics has emerged as an important topic with relevance to a wide array  
40 of climate and ecological research including regional and global carbon modeling,  
41 ecological assessment, and agricultural monitoring, to name only a few (Asner et al.  
42 2000; Lucht et al. 2002; Parmesan and Yohe 2003). At the ecosystem-level, there is  
43 significant history of the use of remotely-derived vegetation indices to monitor  
44 vegetation (e.g., Tucker et al. 1991; Reed et al. 1994; Jia et al. 2003; Zhang et al. 2003;  
45 Reed 2006; Zhang et al. 2006). Common multispectral vegetation indices, such as the  
46 Normalized Difference Vegetation Index (NDVI, Tucker 1979) and the Enhanced  
47 Vegetation Index (EVI, Huete et al. 2002), exploit the difference in visible and near-  
48 infrared (NIR) reflectance due to the presence of chlorophyll. These indices only  
49 provide information about the green (or photosynthetic) portion of terrestrial  
50 vegetation.

51 Though green vegetation (GV, sometimes also called photosynthetic vegetation, PV) is  
52 undoubtedly a critical component of vegetation dynamics, it is not the only component.  
53 Nonphotosynthetic vegetation (NPV), whether standing live material, standing  
54 senescent material, or litter is a key element of many terrestrial ecosystems (e.g.,  
55 Roberts et al. 1993; Asner and Heidebrecht 2002; Elmore et al. 2005; Guerschman et al.  
56 2009). For instance, NPV provides vertical structure in ecosystems, large amounts of  
57 carbon is stored in living and dead NPV, and NPV (particularly dead) is susceptible to  
58 fire. Bare ground cover is a critical element of terrestrial ecosystems as well, with  
59 important controls on albedo and erosion (e.g, Warren and Hutchinson 1984; Balling  
60 1988; Kleidon et al. 2000; Lopez et al. 2000; Nicholson 2000; Bonfils et al. 2001).

61 Thus, value can be added to remote sensing studies of the Earth's ecosystems by  
62 incorporating information on NPV dynamics. The Cellulose Absorption Index (CAI)  
63 (Nagler et al. 2003) has been suggested as one method, though this approach relies on  
64 several relatively narrow spectral bands in the short-wave infrared (SWIR) that are  
65 usually provided by hyperspectral imagery. To date, there are few methods for retrieval  
66 of NPV dynamics from multispectral imagery. Guerschmann et al. (2009) found that a  
67 combination of NDVI and a ratio of Moderate Resolution Imaging Spectrometer  
68 (MODIS) reflectance bands could be empirically calibrated against CAI values to yield  
69 time series of NPV cover that showed agreement with field data. This approach is not  
70 theoretically based.

71 One problem with the retrieval of NPV cover information from coarse spectral  
72 resolution remote sensing data is its spectral similarity to soil; the spectral variance of  
73 these two endmembers overlaps (Okin 2007). In the visible and NIR portions of the  
74 spectrum, both typically have increasing reflectance with increasing wavelength with  
75 few strong spectral absorption features. In the SWIR spectral region from 2 - 2.5  $\mu\text{m}$ ,  
76 NPV and soil can have distinctive absorption features that can be discerned using high  
77 spectral resolution. In NPV, these are due to C-H, N-H, and C-O vibrations in starches  
78 and sugars (Curran 1989) and in soils these are typically due to Al-OH or metal-OH  
79 vibrations in minerals (Clark et al. 1990). However, these features, as well as the  
80 tendency of absorption to decrease in both minerals and NPV with increasing  
81 wavelength in the SWIR, mean that it can be difficult to separate soil and NPV using  
82 coarse spectral resolution imagery such as MODIS or TM/ETM+ without knowledge of at  
83 least one component. In contrast, the characteristic spectrum of GV with strong

84 absorption in the visible, high reflectance in the NIR and characteristic water  
85 absorption features throughout the infrared makes GV easy to separate spectrally from  
86 both NPV and soil (Curran 1989). The usual strong difference in reflectance between the  
87 red and NIR wavelengths is the basis of many indices of GV cover that can be used with  
88 coarse spectral resolution data (e.g., Huete et al. 2002).

89 Spectral mixture analysis (SMA) and its derivatives provide another promising avenue  
90 for retrieval of NPV and soil cover from multispectral imagery (e.g., Asner and  
91 Heidebrecht 2002; Ballantine et al. 2005; Elmore et al. 2005), however most SMA  
92 techniques require knowledge of the spectrum of the soil background. The spectra of  
93 soils, in turn, are highly diverse depending on mineral content, organic matter content,  
94 soil texture, and the presence of crusts (e.g., Gerbermann 1979; Price 1990; Franklin et  
95 al. 1993; Ben-Dor and Banin 1994; Palacios-Orueta and Ustin 1998; Karnieli et al. 1999;  
96 Chabrillat et al. 2002; Ben-Dor et al. 2003; Okin and Painter 2004). The resultant spatial  
97 variability of soil spectra makes large-scale SMA-based analysis in which knowledge of  
98 the soil spectrum is required extremely difficult. Multiple endmember SMA (MESMA,  
99 Roberts et al. 1998) was developed to accommodate spectral variability in all ground  
100 components, including soil, but requires a large library of endmember spectra. In  
101 contrast, relative spectral mixture analysis (RSMA, Okin 2007) was designed to obviate  
102 the need for a library of soil endmembers, or indeed any soil endmember, while still  
103 providing information on the dynamics of GV, NPV, and soil.

104 Given the difficulty of deriving information on the fractional cover of NPV and soil, the  
105 purpose of this report is to determine how SMA-based indices of GV, NPV, and soil  
106 derived from 500-m MODIS reflectance data perform in relation to *in situ* fractional

107 cover measurements. Because RSMA differs from the other SMA-based methods we also  
108 describe and evaluate a method for calibrating RSMA-based indices to absolute  
109 fractional cover.

## 110 **Methods**

### 111 ***Study area***

112 The study was conducted in a rain-fed cropping region of South Australia with a  
113 Mediterranean climate (Figure 1). The region experiences hot dry summers (December  
114 - February) and mild wet winters (July - August), and receives an average annual  
115 rainfall of approximately 500 mm. Agriculture in the region is dominated by annual  
116 rotations of cereal crops, legumes and rapeseed/canola (*Brassica napu*). Through the  
117 summer, the landscape is largely dry although out of season rainfall can lead to  
118 summer weed and pasture growth that can produce significant GV cover. This is  
119 followed by rainfall in late March through to May and subsequent weed and pasture  
120 growth, until chemical spraying of weeds and seeding, or direct-drill seeding, which  
121 reduce cover to a minimum in May-June. Following seeding, annual crops germinate  
122 and growth peaks in September. Finally crops ripen, senesce and are harvested in  
123 November and December. Stubble remaining after harvest is commonly grazed by stock  
124 throughout summer.

125 This study focuses on nine fields ranging in size from 61 to 257 hectares. These fields  
126 were chosen for their extremely large size, relative uniformity of soil and uniformly flat  
127 topography. This design allowed us to obtain fractional cover from fields corresponding

128 to several MODIS pixels, with reasonable expectation of homogenous soil-cover due to  
129 minimal soil variability and minimal topographic redistribution of rainfall.

### 130 ***In situ fractional cover data***

131 *In situ* fractional cover data were collected on three dates using two survey methods,  
132 one step-point and the other photographic (Table 1). Three dates were sampled to  
133 ensure that a wide range of fractional covers (i.e.,  $f_{GV}$ ,  $f_{NPV}$  and  $f_{Soil}$ ) were characterized.  
134 The April and June survey dates were chosen to capture maximum  $f_{Soil}$ . The October  
135 survey was timed to coincide with the expected time of peak green canopy cover, but  
136 before any crop senescence, to capture maximum  $f_{GV}$ .

137 The step-point method was used on the first two survey dates (April and June) when  
138 crops were either not present, or were so new that little damage was caused. The  
139 photographic method was used on the last field survey dates when crop canopies were  
140 full and green (October). The photographic method was used to minimize crop  
141 disturbance.

### 142 *Step-point method*

143 To record *in situ* fractional cover with our step-point method two surveyors walked  
144 step-point transects (Evans and Love 1957; Mentis 1981) crossing each field from fence  
145 to fence in a “W” pattern. Both surveyors started in the middle of “W” in the middle of  
146 one side fence, and each walked half of the “W”, reaching the opposite fence at the 1/3<sup>rd</sup>  
147 and 2/3<sup>rd</sup> points, then returning towards the starting side and finishing in the field  
148 corners. On every second step (~ 1.5-m intervals) surveyors recorded the cover type  
149 (GV, NPV or soil) directly under a thin line drawn on the end of their shoe. For each



150 field, fractional cover was determined by combining the step-point tallies of both  
151 surveyors, and then calculating the proportion of each cover type out of the combined  
152 tallies. The total number of step-point recordings taken within each field ranged from ~  
153 560 to 2500 depending on field size.

#### 154 *Photographic method*

155 Vertical, nadir-oriented high-resolution color digital photographs were taken from  
156 approximately one meter above the crop canopy. *In situ* fractional cover was  
157 determined by overlaying a regular grid of 100 points (10 x 10) over each photograph,  
158 and visually scoring the cover type at each point as GV, NPV, soil or  
159 shadow/unidentified. For each field, fractional cover was determined by combining the  
160 point tallies from all photographs for that field, excluding shadow/unidentified, and  
161 calculating the proportion of each cover type out of the total tally for that field.

162 Between six and thirty photographs were taken in each field to ensure within-field  
163 variability was adequately captured. Photographs were taken near the corner of each  
164 field, far enough into the crop that no edge effects were visible. If some field corners  
165 were not accessible, they were not sampled. At each corner a short transect was walked  
166 into the field and a photograph was taken every five paces. In fields with more  
167 perceived cover variation more photographs were taken. However, analysis revealed  
168 little variation in cover levels between photographs within each field. The total number  
169 of points assessed from all photographs for each field ranged from 600 to 2500.

170 *Comparison of step-point and photographic method*

171 While the step-point and photographic methods differ, these differences should not  
172 have differentially influenced the measured vegetation cover fractions. Both methods  
173 relied on human visual interpretation of cover type at points, and both methods were  
174 designed to minimize user bias in point placement.

175 ***Field Spectroscopy***

176 Despite the relative uniformity of soils in the study area, soils were still expected to  
177 account for the majority of within-scene spectral variation, with little variation in GV  
178 and NPV spectra. To this end, field spectral collection primarily focused on capturing  
179 the range of present soil spectral variation, and secondarily captured some reference  
180 GV and NPV spectra.

181 Spectra were collected in the field with an Analytical Spectral Devices (ASD) full-range  
182 Fieldspec<sup>®</sup> 4 spectroradiometer (wavelength range 400 – 2,500 nm) contact probe. Prior  
183 to the first spectra collection at each site, and when switching from one cover type to  
184 another at a site the spectroradiometer was optimized and then calibrated to a  
185 Spectralon<sup>®</sup> white reference target.

186 Field spectra were recorded on 21 March 2011, and between 4 and 11 soil spectra were  
187 recorded at each of nine locations covering the two major soil groups present in the  
188 study fields (Figure 2). Between five and seven NPV spectral samples were collected for  
189 each of the three crop residues present in the study fields (lentils, rapeseed and wheat).  
190 As the spectral sampling was conducted very early in the growing season the only  
191 green vegetation present was wheat. Three green wheat spectra were recorded.

192 **Remote Sensing**

193 *MODIS Data*

194 Two MODIS datasets were used in this study. The first was the Terra+Aqua 500-m, 16-  
195 day MODIS Nadir BRDF-Adjusted Reflectance (NBAR) dataset (MCD43A4, NASA Land  
196 Processes Distributed Active Archive Center (LP DAAC) 2001a; Schaaf et al. 2002). The  
197 second was the Terra 500-m 16-day MODIS vegetation index dataset (MOD13A1, NASA  
198 Land Processes Distributed Active Archive Center (LP DAAC) 2001b; Huete et al. 2002),  
199 from which EVI values were extracted. The compositing dates for both datasets are  
200 given in Table 1. Average values for each field for EVI for each compositing period were  
201 extracted for comparison with other estimates of GV dynamics.

202 *SMA and MESMA*

203 In SMA, the apparent surface reflectance is assumed to be a linear combination of the  
204 reflectance of the spectra of the ground components, “endmembers”, weighted by their  
205 fractional cover in each pixel. The SMA equation for  $n$  endmembers at time  $t_i$  is:

206 
$$\rho_{pixel}^{t_i} = \sum_{k=1}^n f_k^{t_i} \rho_k + \varepsilon, \quad (1)$$

207 where  $\rho_{pixel}^{t_i}$  is the reflectance of the pixel at time  $t_i$ ,  $\rho_k$  is the reflectance of the  $k$ -th  
208 endmember, and  $f_k^{t_i}$  is the fractional area covered by the  $k$ -th endmember at time  $t_i$   
209 (Shimabukuro and Smith 1991). When derived from laboratory or field spectra,  $\rho_k$  are  
210 sometimes called “reference endmembers” (Roberts et al. 1998). The final term,  $\varepsilon$ , is the  
211 residual spectrum remaining after best-fit coefficients,  $f_k^{t_i}$ , have been determined.

212 Equation (1) is sometimes subject to the constraints that  $f_k$  must belong to the interval  
213 [0,1] and

$$\sum_{k=1}^n f_k = 1 . \quad (2)$$

215 SMA assumes that the reference endmembers are spatially invariant. Use of SMA in the  
216 context here, where the same endmembers are used to unmix images from different  
217 times further requires the assumption that the endmembers are temporally invariant.

218 MESMA is a version of SMA in which the best-fit coefficients of many different SMA  
219 models (a model is a unique combination of endmember spectra) are calculated and the  
220 best model is picked among these (Roberts et al. 1998). One criterion often used in  
221 MESMA to pick the best model is  $RMSE_S$ :

$$RMSE_S = \left( \frac{1}{m} \sum_{b=1}^m (\varepsilon_b)^2 \right)^{1/2} , \quad (3)$$

223 where  $m$  is the number of bands in the remote sensing imagery (MCD43A4 has seven  
224 bands) and the subscript 'S' refers to the RMSE of the spectral fit; The model with the  
225 lowest  $RMSE_S$  is chosen (Roberts et al. 1998). For applications with a large number of  
226 bands, such as those using hyperspectral data, other criteria can be used (e.g., Roberts  
227 et al. 1997; Dennison et al. 2004). Endmember spectra used for MESMA analysis are  
228 shown in Figure 2. Collection of field spectra used as endmembers for MESMA is  
229 discussed above. Models were constructed by using all possible combinations among  
230 three GV spectra, nine NPV spectra, and 38 soil spectra resulting in 1,026 total models.

231 Examination of the MESMA results for the area containing our fields showed that only  
232 three models were used to model the field area, with one model being by far the  
233 dominant. All of these models contained the same GV and NPV spectra and differed  
234 only in their soil spectra. The GV and NPV spectra that were used by MESMA in the best  
235 models of our fields were used as endmembers in the SMA unmixing as was the soil  
236 spectrum from the dominant model (Figure 2).

237 Any spectrum can be used as an endmember, though each cover type can be  
238 represented only once, and we wished to use the most spectrally representative field  
239 spectra in our SMA unmixing. Given the high variability in measured field spectra even  
240 over a small area, no endmember spectrum can be identified as the most representative  
241 *ab initio*, particularly in light of the impact of vegetation structure on what MODIS  
242 ultimately sees. The use of the spectra that resulted in the lowest residual error, in a set  
243 of MESMA models where all combinations are tried, guarantees that SMA will provide  
244 the lowest possible residual errors as well. However, selection of SMA endmembers in  
245 this way probably optimizes the ability of SMA to capture fractional cover, compared to  
246 an approach where SMA endmembers are chosen without guidance based on how well  
247 they fit the image spectra.

248 For both SMA and MESMA, unmixing was conducted using the “constrained\_min”  
249 routine in IDL (Excelis Visual Information Solutions, inc., Boulder, Colorado; Lasdon and  
250 Waren 1986) to minimize RMSE while forcing coefficients to exist in the interval [0,1].  
251 The advantage to this approach compared to another linear unmixing method using  
252 linear algebraic least-squares analysis (including a QR decomposition using the Gram-  
253 Schmidt process or the use of singular value decomposition (SVD)) is that constraints

254 can be strictly enforced; values outside [0,1] can be avoided if desired. Roberts et al.  
255 (1998), using a least-squares mixing approach based on a QR decomposition using  
256 Gram-Schmidt orthogonalization, for instance, allowed endmembers to be slightly  
257 outside the [0,1] constraints. In cases where there exists a solution for the endmembers  
258 that falls within the constraints, both the method used here and a linear algebraic least-  
259 squares will provide the same solution.

260 Two sets of SMA and MESMA fractional cover estimates were included in our analysis.  
261 In the first, no constraint on the sum of non-shade endmembers was imposed. This  
262 method is equivalent to that used in Roberts et al. (1998). In that study, the constraint  
263 that all endmembers sum to one is imposed by inferring an additional photometric  
264 shade endmember (zero reflectance in all bands) that is not used in the actual  
265 unmixing. The fractional cover of the photometric shade endmember is set to one  
266 minus the sum of the other endmember fractions. This approach is required because  
267 photometric shade cannot be used directly as an endmember in a spectral mixture  
268 model. Depending on the algorithm used for estimation of fractions (i.e.,  $f_k$ ) several  
269 undesirable outcomes result with the inclusion of photometric shade directly. For  
270 instance: 1) using simple linear least squares, the  $X^T X$  matrix, where  $X$  is a column  
271 vector containing endmembers, is not invertible, 2) a least squares approximation  
272 using QR decomposition employing the Gram-Schmidt process results in non-real  $Q$  and  
273  $R$  matrix values, 3) least squares estimation using singular value decomposition (SVD)  
274 results in the shade fraction always being equal to zero, and 4) the heuristic  
275 constrained\_min algorithm based on gradient reduction used here results in unstable  
276 shade fractions (i.e., subsequent calculations do not result in the same shade fraction).

277 In the first two cases, the failure occurs because the photometric shade is a linear  
278 combination of any/all of the other spectra through multiplication by zero, a condition  
279 that is prohibited in these methods.

280 In the second set of fractional cover estimates, best-fit coefficients for a pixel were  
281 divided by the sum of all best-fit (non-shade) coefficients for that pixel, thus ensuring  
282 that the fractional cover estimates summed exactly to one. This method more closely  
283 matches treatment of *in situ* data, in which the sum of GV, NPV, and soil points were  
284 used to normalize GV, NPV and soil fractions, thus ignoring shade points.

285 RSMA

286 As originally published, RSMA used four endmembers to unmix pixel spectra: a baseline  
287 spectrum, a GV spectrum, an NPV spectrum, and a snow spectrum (Okin 2007). Since  
288 snow does not fall in the study area the snow endmember was omitted from this  
289 analysis. In RSMA, the apparent surface reflectance for a pixel at a reference time,  $t_0$ , in  
290 a timeseries of collocated images is defined as the “baseline” spectrum of that pixel,  $\rho_B$ .  
291 From Equation 1, the baseline spectrum can be modeled (assuming, in this case, no  
292 snow) as:

$$293 \quad \rho_B = f_{GV}^{t_0} \rho_{GV} + f_{NPV}^{t_0} \rho_{NPV} + f_{soil}^{t_0} \rho_{soil} . \quad (4)$$

294 The reflectance of the soil background,  $\rho_{soil}$ , is assumed to vary spatially and is assumed  
295 to be unknown.  $f_{GV}^{t_0}$ ,  $f_{NPV}^{t_0}$ , and  $f_{soil}^{t_0}$  (i.e., the fractional area of the ground  
296 components at time  $t_0$ ) are also assumed to be unknown. The spectra of the ground  
297 components,  $\rho_{GV}$ ,  $\rho_{NPV}$ , and  $\rho_{soil}$ , are assumed to be invariant with time.

298 The assumption that the soil spectrum is constant with time over a MODIS pixel and  
299 compositing period is justifiable, particularly in arid areas. In a sandy soil, light from  
300 the sun only penetrates about four sand grains (i.e. a few millimeters) into the soil  
301 (Okin et al. 2001). In heavier textured soils, this distance will be smaller due to more  
302 efficient scattering by small particles (Hapke 1981). Thus, though soil moisture does  
303 reduce soil reflectance by changing the index of refraction of the medium in soil pores,  
304 once the top several particles are back into equilibrium with the (dry) atmosphere,  
305 reflectance will return to its pre-wetting value (Lobell and Asner 2002). This happens in  
306 arid areas, including our field site, quite quickly after wetting. A back of the envelope  
307 calculation using the data of Lobell and Asner (2002) assuming a constant evaporation  
308 equal to the potential evapotranspiration of  $1 \text{ m yr}^{-1}$  in the field area (Chiew et al. 2002),  
309 shows that even saturated soils will return to near-original reflectance in significantly  
310 less than one day. This time is short compared to the compositing time of the MODIS  
311 data, effectively minimizing the impact of wetting events on reflectance. Even if soil  
312 moisture variability were to have a significant effect on the variability of the soil  
313 spectrum in MODIS images, at the coarse spectral resolution of MODIS the main impact  
314 of wetting is to reduce the total reflectance rather than significantly change the shape  
315 of the soil spectrum. Besides changes in soil surface moisture, other changes to the soil  
316 that would cause a considerable change in soil reflectance either occur over very long  
317 times compared to the period of this research (i.e., weathering, oxidation, growth of a  
318 biological crust, winnowing, or development of a lag gravel) or occur over very small  
319 areas compared to the size of a MODIS pixel (i.e. development of a trail, track, or road  
320 from foot or vehicular traffic).



321 The spectrum of vegetation in RSMA can change through time, but is modeled at all  
 322 times as a linear combination of invariant GV and NPV spectra, always chosen (as in,  
 323 Okin 2007) to be very green (full canopy of green grass) and very brown (full canopy of  
 324 dry/senescent grass) spectral endmembers. Although there is a considerable amount of  
 325 variation in vegetation spectra, the shape of the very “green” and very “brown”  
 326 examples have a remarkable degree consistency, particularly in coarse resolution  
 327 remotely sensed data, such as MODIS (e.g., Figure 2, Asner and Heidebrecht 2005). Thus,  
 328 the assumption of invariant GV and NPV spectra used in RSMA as endmembers for the  
 329 modeling of pixel-wide vegetation at any phase of greenness/brownness is a strong  
 330 assumption that allows RSMA to elicit temporally and spatially consistent timeseries of  
 331 GV, NPV, and soil dynamics (Okin 2010). This is particularly the case here, where the  
 332 crop species on the target fields (cereal crops, legumes and rapeseed/canola) exhibit  
 333 typical green and brown spectra during their growing and senescent phases,  
 334 respectively (e.g, Figure 2, Nagler et al. 2000; Nagler et al. 2003; Nidamanuri and Zbell  
 335 2011). Thus, the original RSMA spectra (Okin 2007) are not only very close to those  
 336 found in the field area, but their use allows us to maintain consistency with earlier  
 337 applications of RSMA.

338 In RSMA, the apparent surface reflectance of a pixel at time  $t_i$ , is modeled as:

$$339 \quad \rho_{pixel}^{t_i} = x_{GV}^{t_i} \rho_{GV} + x_{NPV}^{t_i} \rho_{NPV} + x_B^{t_i} \rho_B + \varepsilon, \quad (5)$$

340 where,

$$341 \quad x_{GV}^{t_i} + x_{NPV}^{t_i} + x_B^{t_i} = 1. \quad (6)$$

342 The terms  $x_B$ ,  $x_{GV}$ , and  $x_{NPV}$  replace the more familiar fractional area terms (denoted as  $f$   
343 in Equation (1)) in SMA.  $x_{GV}$ ,  $x_{NPV}$ , and  $x_B$  are hereafter called RSMA “indices” because  
344 they provide an index of the change of these groundcover components from the  
345 reference time without providing actual fractional cover values. Values of  $x_{GV}$  and  $x_{NPV}$   
346 can be positive or negative.  $x_B$  can be shown to be the ratio of the non-vegetation  
347 (interpreted as soil) fractional cover at time  $t_i$  to the non-vegetation fractional cover at  
348 time  $t_o$ , and therefore varies around one rather than zero, like  $x_{GV}$ ,  $x_{NPV}$ . Values of  $x_{GV}$ ,  $x_{NPV}$ ,  
349 and  $x_B$  are the best-fit coefficients for Equation (5) that minimize the RMSE calculated  
350 using Equation 3. The GV and NPV spectra originally published in Okin (2007) were  
351 used here (Figure 2). Unmixing was conducted using the “la\_least\_square\_equality”  
352 routine in IDL (Excelis Visual Information Solutions, inc., Boulder, Colorado; Anderson  
353 et al. 1999), which minimizes squared error and forces the coefficients to sum to one.  
354 The advantage to this approach compared to another linear unmixing method using  
355 linear algebraic least-squares analysis (including a QR decomposition using the Gram-  
356 Schmidt process or the use of singular value decomposition (SVD)) is that constraints  
357 can be strictly enforced; in particular, the sum of fractions can be forced to equal  
358 exactly one. In cases where there exists a solution for the endmembers that falls within  
359 the constraints, both the method used here and a linear algebraic least-squares will  
360 provide the same solution.

### 361 *Calibration of RSMA to absolute cover values*

362 RSMA index values are related to the *difference* between the cover of a ground cover  
363 component at time  $t_i$  and the cover of a ground cover component at  $t_o$ , the reference  
364 time (Okin 2007). RSMA index values, as differences, should therefore be directly

365 relatable to the difference in the measured cover between time  $t_i$  and  $t_o$ . This logic  
366 provides a means to calibrate RSMA index values to absolute cover estimates, to wit:

$$367 \quad Y_j^{t_i} = x_j^{t_i} M_j + B_j + f_j^{t_i}, \quad (7)$$

368 where  $Y_j^{t_i}$  is the array of empirically corrected RSMA indices of ground component,  $j$   
369 (GV, NPV, or soil). Values of  $Y_j^{t_i}$  can be interpreted as estimates of absolute cover at  
370 some time ( $t_i \neq t_o$ , *sensu* Equations 4 and 5).  $x_j^{t_i}$  is the array of original RSMA index values  
371 at  $t_i$  of ground component  $j$ .  $f_j^{t_i}$  is the array of *in situ* fractional cover estimates of  
372 ground component  $j$  at the reference time,  $t_o$ .  $M_j$  and  $B_j$  are the slope and intercept for  
373 ground cover component  $j$  of the least-squares linear regression:

$$374 \quad (f_j^{t_i} - f_j^{t_o}) = M_j x_j^{t_i} + B_j + \varepsilon, \quad (8)$$

375 where  $f_j^{t_i}$  is the array of *in situ* fractional cover estimates at time  $t_i$ , and  $\varepsilon$  is the fitting  
376 error.

377 In practice, to avoid the use of training data in estimation of the cover estimated  
378 provided by this method, a leave-one-out approach was used. The procedure given in  
379 Equations (7) and (8) was used nine times. Each time, data from a different field were  
380 left out of the calculations. The mean and standard deviation of the slopes, intercepts,  
381 and correlations (i.e.,  $\sqrt{R^2}$ ) were reported. RMSE was calculated using actual fractional  
382 cover values and predicted fractional cover values from the omitted fields.

383 *Comparison with in situ data*

384 To determine the degree to which remote sensing indices or estimated cover values  
385 agree numerically with *in situ* data, we calculated linear regression relationships  
386 between remotely-sensed values and *in situ* values. In this analysis, remotely-sensed  
387 values were treated as the independent variable and *in situ* values were treated as the  
388 dependent variable. Error in remote sensing estimates of fractional cover were  
389 calculated using two metrics,  $RMSE_c$  and mean absolute error ( $MAE_c$ ):

$$390 \quad RMSE_c = \left( \frac{1}{n} \sum_{i=1}^n \left( f_j^t(i,rs) - f_j^t(i,insitu) \right)^2 \right)^{1/2}, \quad (9)$$

391 and

$$392 \quad MAE_c = \frac{1}{n} \sum_{i=1}^n \left( f_j^t(i,rs) - f_j^t(i,insitu) \right), \quad (10)$$

393 where  $n$  is the number of fields (9) times the number of dates for which cover was  
394 estimated (3),  $f_j^t(i,insitu)$  is the *in situ* estimate of fractional cover for the  $j$ th  
395 endmember at time  $t_i$  for the  $i$ th field-date combination,  $f_j^t(i,rs)$  is the remote sensing  
396 estimate of fractional cover for the  $j$ th endmember at time  $t_i$  for the  $i$ th field-date  
397 combination, and the subscript 'c' refers to the error in fractional cover (to  
398 differentiate from the spectral fitting error in Equation (3)).

399 For the pooled regression and error analysis, the RSMA index  $x_B$ , which naturally varies  
400 around one, was replaced by  $x_B - 1$  so that it would vary around zero as the others do.

401

## 402 Results

403 *In situ* estimates of  $f_{GV}$ ,  $f_{NPV}$  and  $f_{soil}$  followed the expected temporal patterns (Table 2). In  
404 April (mid-Autumn), fields were dominated by crop residues resulting in high  $f_{NPV}$ ,  
405 while summer weeds provided some  $f_{GV}$ . In some fields, low crop-residue retention or  
406 extensive utilization of crop residues lead to high  $f_{soil}$ . In June (winter), all fields had  
407 been cultivated and crop germination resulted in a mixture of low to moderate  $f_{GV}$ ,  $f_{NPV}$   
408 and  $f_{soil}$ . The October survey was timed to coincide with the expected period of  
409 maximum green crop canopy density and recorded universally high  $f_{GV}$ . The average  
410 fraction of shade from photographs in the October survey was 2%.

411 On average, MESMA fit the MODIS reflectance spectra with  $RMSE_s = 2\%$  (reflectance  
412 units), better than SMA ( $RMSE_s = 3\%$ ) and RSMA ( $RMSE_s = 6\%$ ). Since normalization was  
413 conducted after unmixing MODIS, the  $RMSE_s$  must also be calculated *post hoc*. To do  
414 this, MODIS reflectance can be predicted using the normalized SMA and MESMA  
415 fractions and using this prediction to estimate  $RMSE_s$ . This procedure results in  $RMSE_s$   
416 = 15% for normalized SMA and  $RMSE_s = 10\%$  for normalized MESMA.

417 To determine the extent to which remote sensing indices or estimated cover values  
418 agree with each other, regardless of *in situ* data, we calculated correlation coefficients  
419 amongst the different techniques (Tables 3 and 4). All correlations were statistically  
420 significant ( $\alpha=0.01$ ,  $n=26$ ,  $rcrit=0.496$  Rohlf and Sokal 1981) at  $\geq 0.99$ ,  $\geq 0.91$ , and  $\geq 0.73$  for  
421 GV, NPV, and soil, respectively. The worst correlations were for soil cover between  
422 MESMA (both normalized and non-normalized) and RSMA (both  $r \geq 0.73$ ). MESMA (both  
423 normalized and non-normalized) also shows some disagreement with SMA (both

424 normalized and non-normalized) with  $r$  between 0.80 and 0.85. A pooled analysis  
425 looking simultaneously at all ground components (ie., bottom quadrant in Table 3) also  
426 shows a significant correlation ( $r \geq 0.91$ ) for all methods. This analysis could not be  
427 conducted including RSMA. Since the RSMA index values can be either positive or  
428 negative, depending on whether the fractional coverage has increased or decreased  
429 since the reference time, whereas fractional cover values from the other remote  
430 sensing methods will always be positive, pooled correlation between RSMA indices and  
431 other methods do not provide any information about the relative performance of RSMA  
432 with other methods and were not calculated.

433 For methods that directly provide estimates of absolute fractional cover of ground  
434 components (SMA, normalized SMA, MESMA, and normalized MESMA), root mean  
435 squared difference (RMSD, calculated in the same fashion as Equation (9)) and mean  
436 absolute difference (MAD, calculated in the same fashion as in Equation (10)) were  
437 calculated between all methods (Tables 3 and 4). Here, “difference” replaces “error”  
438 because neither of the methods is privileged. EVI and RSMA, because they provide only  
439 indices, cannot be used to calculate RMSD or MAD with other indices or estimates of  
440 cover. RMSD provides information about how different the estimates were, whereas  
441 MAD provides information on the bias in the estimates. For simplicity, only the sign of  
442 MAD is reported. For GV, RMSD shows that SMA and MESMA provided nearly the same  
443 estimates (RMSD=0.01) and normalized SMA and normalized MESMA provided nearly  
444 the same estimates (RMSD=0.05). RMSD is 0.24 – 0.25 when normalized and non-  
445 normalized methods are compared. For NPV, MESMA and normalized SMA provide the  
446 closest estimates (RMSD=0.06) while SMA and MESMA provide the next closest

447 (RMSD=0.11) and the other comparisons yield RMSD > 0.14. For soil, the closest  
448 estimates are provided by SMA and MESMA (RMSD=0.08) and normalized MESMA and  
449 MESMA provide the next closest estimates (RMSD=0.12). For the pooled comparison,  
450 the closest estimates are provided by SMA and MESMA (RMSD=0.08) and normalized  
451 SMA and MESMA provide the next closest estimates (RMSD=0.12).

452 MAD indicates for all cover types (and the pooled analysis) that normalized SMA and  
453 MESMA cover estimates are greater than their non-normalized counterparts (Tables 3  
454 and 4). This result is the direct consequence of the normalization process, where  
455 fractional cover values are multiplied by a factor  $\geq 1$ .

456 Remotely-sensed indices of GV, NPV, and soil (EVI is an index of GV cover, RSMA  
457 provides indices of GV, NPV, and soil) and estimates of fractional cover of these ground  
458 cover components (SMA and MESMA) followed very similar temporal patterns as *in situ*  
459 estimates (Figure 3). Plots of index/cover values vs. *in situ* data (Figure 4) show strong  
460 linear relations between remote sensing methods and *in situ* data.

461 The relationship between RSMA indices and *in situ* fractional cover should be linear,  
462 and for this reason, the correlation between RSMA indices and *in situ* data is the  
463 correct basis of comparison. On this basis, the RSMA soil index actually has the highest  
464 correlation with soil cover of all methods (0.92, Table 5). Other correlations between  
465 remotely-sensed and *in situ* ground cover component estimates were best for GV (  $\geq$   
466 0.94), compared to NPV (  $\geq 0.89$ ) and soil (  $\geq 0.84$ ) (Table 5), and all correlations between  
467 remotely-sensed and *in situ* estimates were significant ( $\alpha=0.01$ ,  $n=26$ ,  $r_{crit}=0.496$  Rohlf  
468 and Sokal 1981). A pooled analysis looking simultaneously at all ground components

469 (ie., “Pooled” in Table 5) also shows a significant correlation ( $r \geq 0.78$ ) for all methods.  
470 The relatively low pooled correlation for RSMA results from the fact that RSMA index  
471 values can be either positive or negative, depending on whether the fractional coverage  
472 has increased or decreased since the reference time, whereas fractional cover values  
473 from the other remote sensing methods will always be positive. Therefore, pooling all  
474 of the cover types results in the superposition of lines that do not, and should not, all  
475 have the same intercept. For example, the fields during the time of reference image  
476 (DOY 113, 2010; April 27, 2010) had the lowest  $f_{GV}$  and the highest  $f_{NPV}$  compared to the  
477 other two dates. Therefore  $x_{GV}^i$  will be positive for the other two dates (i.e., higher  
478 than the reference time) and  $x_{NPV}^i$  will be negative for the other two dates. In contrast,  
479  $f_{GV}^i$  and  $f_{NPV}^i$  are always positive. Thus, even though the  $x_{GV}^i$  vs.  $f_{GV}^i$  and  $x_{NPV}^i$  vs.  
480  $f_{NPV}^i$  relationships have high correlations, the correlation when the GV and NPV  
481 points are considered together must be lower because the intercepts of for GV and NPV  
482 are different.

483 For RSMA, a slightly different correlation analysis was also examined. Because RSMA is  
484 a relative index, the average correlation for all fields between RSMA timeseries and *in*  
485 *situ* fractional cover estimates is instructive (n=3 for these correlations for the three  
486 dates at which the fields were measured). These values are not amenable to statistical  
487 test, but are nonetheless high: 0.99, 0.93 and 0.94 for GV, NPV, and soil, respectively.  
488 This same method could have been used for other remote sensing cover estimates, but  
489 is not necessary since other methods aren’t relative but absolute.



490 Normalized SMA and normalized MESMA had regression slopes closest to one for GV  
491 and NPV excluding residual-corrected RSMA (which is forced to have slopes and  
492 intercepts of regression of one and zero, respectively) (Table 5). When considering the  
493 slope of the relationship for soil, simple (i.e. non-normalized) SMA and MESMA  
494 outperformed their normalized counterparts (i.e., had slopes closer to one). This  
495 pattern is also reflected in  $RMSE_c$  (Table 6). Normalized SMA and normalized MESMA  
496 had the lowest  $RMSE_c$  for GV (0.08 and 0.07, respectively). For NPV,  $RMSE_c$  was higher,  
497 though normalized SMA and normalized MESMA had the lowest  $RMSE_c$  (0.17 and 0.12,  
498 respectively). Non-normalized SMA and MESMA outperformed their counterparts in  
499 terms of  $RMSE_c$  of soil cover (0.07 and 0.08).

500 SMA and MESMA exhibited negative values of  $MAE_c$  for all cover types (Table 6),  
501 indicating that predicted fractional cover was on average lower than *in situ* fractional  
502 cover. This is true for all dates (not shown). For GV, normalized SMA predictions were  
503 unbiased and  $MAE_c$  was only slightly negative for normalized MESMA. For NPV,  
504 normalized SMA and MESMA resulted in negative values of  $MAE_c$  but positive values of  
505  $MAE_c$  were observed for normalized SMA and MESMA soil fractions. In the pooled data,  
506 the positive and negative biases for normalized SMA and MESMA cases canceled each  
507 other out, resulting in no net bias.

508 Calibration of RSMA data to fractional cover using the procedure discussed above (i.e., a  
509 leave-one-out implementation of Equations (7) and (8)) was conducted. For GV and  
510 NPV, correlations between calibrated RSMA values and actual cover values were lower  
511 than all other methods (Table 5). For soil, the correlation coefficient was equal to the  
512 minimum for all other methods. Variation in slope and intercept estimates for GV and

513 soil was very small (Table 6), and it was slightly greater for NPV, reflecting the higher  
514 variance (and lower correlation) seen with this ground component. For the pooled  
515 analysis of all fractional cover, calibrated RSMA had the second highest (0.93 vs. 0.94 for  
516 MESMA) correlation, the slope closest to one (0.93) and the lowest intercept (0.03). This  
517 procedure resulted in unbiased (i.e.,  $MAE_c = 0$ ) estimates of fractional cover.  $RMSE_c$  of  
518 calibrated RSMA values with *in situ* values were comparable to those from other  
519 methods, with values intermediate to the values from other methods. That is to say, the  
520 calibrated RSMA in some cases performed better than SMA and MESMA, and sometimes  
521 worse. In the pooled case,  $RMSE_c$  for calibrated RSMA was second lowest (0.13 vs. 0.11  
522 for MESMA).

523 A unique aspect of our *in situ* data is that they were acquired over three different dates.  
524 The MODIS data are multitemporal as well. This allows an analysis not only of the  
525 absolute index values and fractions, but also their change as well. For RSMA and  
526 calibrated RSMA, these comparisons are one and the same because RSMA provides  
527 information on the changes in fraction from the reference time. For GV, correlation  
528 between  $\Delta(EVI)$  and  $\Delta(f_{GV})$  was highest (0.97) and that between  $\Delta(\text{normalized SMA})$  and  
529  $\Delta(f_{GV})$  was lowest (0.94) with all others being equal (0.96) (Table 5, bottom). For NPV,  
530  $\Delta(\text{RSMA})$  had the lowest correlation with  $\Delta(f_{NPV})$ , whereas  $\Delta(\text{MESMA})$  had the highest  
531 correlation with  $\Delta(f_{NPV})$ . For soil,  $\Delta(\text{RSMA})$  had the highest correlation with  $\Delta(f_{NPV})$ ,  
532 whereas  $\Delta(\text{SMA})$  had the lowest correlation with  $\Delta(f_{NPV})$ . For the pooled analysis  
533  $\Delta(\text{normalized MESMA})$  exhibited the best correlation with changes in field fractional  
534 cover, whereas  $\Delta(\text{RSMA})$  exhibited the lowest correlation. Of all relationships, only the

535  $\Delta(f_{soil})$  vs  $\Delta(\text{RSMA})$  comparison yielded a relationship that fell very near the 1:1 line ( $m =$   
536  $0.99$ ,  $b = 0.02$ ), with the  $\Delta(f_{GV})$  vs.  $\Delta(\text{Normalized SMA})$  exhibiting a slope near one, but  
537 with considerable overprediction ( $\text{MAE}_c = 0.10$ , consistent with  $m < 1$  and  $b < 0$  for the  
538  $\Delta(f_{GV})$  vs.  $\Delta(\text{Normalized SMA})$  line).

539 For GV, the smallest bias ( $\text{MAE}_c$ ) and lowest error ( $\text{RMSE}_c$ ) was observed for  
540  $\Delta(\text{Normalized MESMA})$ , whereas  $\Delta(\text{MESMA})$  had the lowest error for NPV and soil  
541 (Table 6, bottom).  $\Delta(\text{Normalized MESMA})$  exhibited the least biased estimates of  $\Delta(f_{NPV})$   
542 and  $\Delta(\text{SMA})$  exhibited the least biased estimates of  $\Delta(f_{soil})$ . Overall, biases for all methods  
543 were low ( $\text{MAE}_c = -0.01 - 0.0$ ) and errors were nearly equal ( $\text{RSMA}_c = 0.17$  for all except  
544  $\Delta(\text{SMA})$  with  $\text{RSMA}_c = 0.20$ ).

## 545 Discussion

546 In this study, we compared several methods for use with MODIS NBAR data that can be  
547 used either to produce indices of change in GV, NPV and soil (EVI, RSMA) or to produce  
548 absolute estimates of these ground cover components. Our results did not indicate that  
549 a single technique worked best in all circumstances, particularly when bias ( $\text{MAE}_c$ )  
550 absolute error ( $\text{RMSE}_c$ ) were considered.

551 Comparisons amongst remote sensing methods (Tables 3 and 4) are informative. The  
552 information content of the remote sensing imagery used to produce indices or  
553 fractional cover estimates of GV, NPV, and soil is the same because the imagery is all  
554 the same. In the case of RSMA, SMA, and MESMA, the same NBAR data was used as  
555 input in our calculations. EVI is also produced from this NBAR data, though we  
556 downloaded the MODIS product rather than calculating it ourselves. Given the same

557 input data, then, comparisons amongst results from different methods provide  
558 information on the inherent differences amongst the analytical methods, regardless of  
559 *in situ* data. The results in Tables 3 and 4 therefore provide benchmarks against which  
560 comparisons with *in situ* data can be made. *In situ* data carry their own estimation  
561 errors and biases and it is unreasonable to expect that comparisons with *in situ* data  
562 yield better relationships than comparisons amongst remote sensing techniques; since  
563 they use the same input data (i.e., imagery), data-related errors and bias are consistent  
564 among remote sensing methods.

565 The source of disagreement (i.e., high RMSD despite high correlation) between  
566 normalized and non-normalized versions of SMA and MESMA are clear; normalization  
567 systematically changes fractional cover estimates so even if SMA and MESMA provide  
568 the same estimates of fractional cover (i.e., low RMSD), normalization will increase  
569 RMSD when comparing normalized and non-normalized versions of the same  
570 technique. This effect is visible in all cover types as well as the pooled data (Table 3).  
571 In the pooled data, for instance, the lowest RMSDs are 0.08 and 0.12, respectively, for  
572 the SMA-MESMA and Normalized SMA-Normalized SMA comparison (i.e., apples-to-  
573 apples comparisons vis a vis normalization). Thus, if the values of RMSD are used as a  
574 benchmark for the pooled data, we would not expect  $RMSE_c$  values to be lower than  
575 0.08-0.12. Indeed, the lowest  $RMSE_c$  is 0.11 (for MESMA), which is comparable to the  
576 lowest RMSDs. (0.08 – 0.12).

577 For pooled data, this suggests that  $RMSE_c$  is as low as can be expected, suggesting that  
578 MESMA is giving the best possible pooled estimates of cover. The situation is somewhat  
579 different when examining individual cover types. For GV, the lowest  $RMSE_c$  is seven

580 times the lowest RMSD (0.07 vs. 0.01), suggesting that even though GV estimates are  
581 better than the other cover types, they are far from what they could be optimally. On  
582 the other hand, the lowest  $RMSE_c$  for soil is approximately equal to the lowest RMSD  
583 ( $RMSE_c = 0.07$  for SMA vs.  $RMSD = 0.08$ ) suggesting that soil retrievals for SMA are as  
584 good as they are likely to get, at least using the set of endmembers employed here.

585 Comparisons between RSMA indices and SMA or MESMA results cannot, unfortunately,  
586 use RMSD because these techniques provide different types of values. For NPV, though,  
587 we see that RSMA index values and fractional cover from the SMA techniques are  
588 highly correlated (Table 4). It is therefore unsurprising that the correlations for all of  
589 these techniques with MESMA data are about the same ( $r = 0.89 - 0.93$ ). The soil results  
590 tell a different story, however. RSMA soil index values and SMA fractional cover values  
591 are highly correlated ( $r = 0.92-0.94$ ), but the correlation between RSMA and MESMA  
592 fractional cover values display a much lower correlation ( $r = 0.73$ ) (Table 4). Indeed, the  
593 SMA and MESMA correlation is also low ( $r = 0.81$ ) indicating some difference between  
594 RSMA/SMA and MESMA. Since the input imagery is the same in all cases, the difference  
595 must be inherent to the techniques themselves. Since the same code was used to  
596 calculate fractions from SMA and MESMA the only possible difference between these  
597 techniques is the availability of additional endmembers in MESMA. However, we see  
598 that the consequence of the availability of additional endmembers is not to improve the  
599 correlation with *in situ* soil fractional cover estimates, because correlation coefficients  
600 are actually higher (and  $RMSE_c$  is lower) for SMA compared to MESMA. It cannot be  
601 assumed that MESMA always makes soil fractional cover estimates better. Okin et al.  
602 (2001) showed that “coupling” between soil and NPV spectra can actually lead to error

603 in MESMA as some combinations of soil/NPV can masquerade as combinations of other  
604 soil/NPV. This question can only be answered by comparing with *in situ* estimates, to  
605 which we now turn.

606 There are features of Figures 3 and 4, which exhibit comparisons between remote  
607 sensing and *in situ* results, that might make the RSMA results misleading. RSMA, unlike  
608 the other methods, provides an index of change relative to some reference time. If, for  
609 example, the fractional cover of NPV is 0.5 at the reference time and also at a later date,  
610 the RSMA NPV index will be zero at that later date despite the non-zero fractional  
611 cover of NPV. Therefore, in a plot against absolute fractional cover from *in situ*  
612 measurements (as in Figure 4), the 1:1 line has no special meaning for the RSMA  
613 indices. Furthermore, the RSMA soil index,  $x_B$ , varies around one rather than zero,  
614 unlike the other RSMA indices. So, while no change in GV and NPV cover from the  
615 reference time would give RMSA GV and NPV index values of zero, no change in soil  
616 cover would give an RSMA soil index value of one. As a result, values of RSMA index  
617 values tend to not cluster with others in Figures 3 and 4 and this difference is especially  
618 glaring for soil

619 As an index of GV change our data suggests that  $x_{GV}$ , from RSMA, and  $f_{GV}$  from SMA and  
620 MESMA are as useful as EVI. The benefit of EVI is its computational simplicity and  
621 availability of a standard MODIS product. The benefit of SMA and MESMA are the fact  
622 that they provide absolute GV cover estimates, though the availability and choice of  
623 endmembers complicates these methods. The benefit of RSMA is that it provided strong  
624 correlations with *in situ* GV cover without the need for additional information (i.e.,  
625 using endmembers that appeared in the original RSMA publication (Okin 2007)), though

626 it can only provide information about the change of GV cover rather than the absolute  
627 fractional cover.

628 However, the development of RSMA was spurred not by the need for another GV index,  
629 but rather by the need for remotely-sensed information about NPV and soil. When soil  
630 fraction less negative soil soil fraction less negative soil at correlations among remotely-  
631 sensed values of NPV, we see greater disagreement than with GV (i.e., lower  
632 correlations). These differences highlight the difficulty extracting information on NPV  
633 from satellite-derived surface reflectance. Nonetheless, the RSMA index of NPV  
634 performs well, and essentially equally, when compared to SMA and MESMA (both  
635 normalized and non-normalized) (Table 5). Retrieval of NPV from reflectance imagery  
636 is made difficult, in part, by the fact that its spectrum can be so similar to that of the  
637 soil, particularly in multispectral imagery (Figure 2 and Okin (2007)). The NPV signal is  
638 therefore subtle in the presence of soil background and the lower correlations for NPV  
639 compared to GV are a likely consequence.

640 The only direct comparison between RSMA indices and *in situ* fractional cover possible  
641 is correlation; there is no reason to expect that the magnitude of absolute RSMA should  
642 match that of fractional cover, just as the magnitude of EVI should not match that of  
643 GV fractional cover. For GV and NPV, the correlations between RSMA indices and *in situ*  
644 fractional cover are high and comparable to those from SMA/MESMA retrieval (0.99 v.  
645 0.99 and 0.89 vs. 0.92-0.93, respectively; Table 5). For soil, the correlation between  
646 RSMA indices (0.92) is greater than that for both normalized and non-normalized SMA  
647 and MESMA (0.84-0.90). These results indicate clearly that RSMA provides information

648 on GV, NPV and soil dynamics similar to those provided by the more traditional SMA  
649 methods

650 A surprising result, despite the simplicity of the RSMA approach and the fact that this  
651 method does not utilize a “soil” spectrum in unmixing, is that this method provides  
652 excellent predictions (with slopes close to 1) of changes in soil cover. Indeed, of all  
653 methods and all cover types, RSMA provides the best prediction of soil cover change  
654 (Figure 5).

655 RSMA was created to provide an index of change of fractional cover ground  
656 components, particularly in cases when the spectrum of the soil background is not  
657 known. SMA and MESMA, in comparison, require knowledge of the soil spectrum and,  
658 in the case of MESMA, several soil spectra to chose from. Indeed, in the results here, we  
659 probably inflated the accuracy of SMA by using for SMA the soil spectrum that most  
660 often modeled our study area using MESMA. The choice of other spectra for SMA  
661 would have changed the accuracy of this approach, but the extent to which alternate  
662 endmember selection improves or degrades accuracy would depend, of course, on the  
663 endmembers actually used.

664 Comparing SMA and MESMA it is interesting to note that normalization did not  
665 uniformly improve (or degrade) the relationship with field data, particularly when  
666 looking at RMSE. In some cases where normalization decreased (increased) RMSE, it  
667 also decreased (increased) the correlation coefficient. For GV, normalization of SMA  
668 decreased RMSE but also slightly reduced the correlation with *in situ* data. For NPV,



669 normalization did not change the correlation coefficient despite lowering RMSE. For  
670 soil, normalization increased RMSE while also increasing the correlation coefficient.

671 This pattern can be explained by analysis of the values of  $MAE_c$ . SMA tends to  
672 underestimate ( $MAE_c < 0$ ) GV and NPV cover significantly. Soil is only slightly  
673 underestimated. This suggests that either 1) the endmembers used in SMA and MESMA  
674 were brighter than the effective spectra of these ground cover components in the  
675 MODIS scenes such that lower fractions of brighter spectra offset one another, or 2)  
676 shade makes up a significant portion of the scene resulting in reduced MODIS-observed  
677 reflectance.

678 Shading of soil by plants would reduce soil fraction and increase GV and NPV fraction  
679 (when all endmembers are divided by the sum of non-shade endmembers, as done  
680 here). This would thus tend to make negative biases of soil fraction less negative and  
681 negative biases of GV and NPV more negative. This might explain, in part, the smaller  
682 biases observed for SMA and MESMA soil fractions compared to those of GV and NPV.

683 Though our point-step methods are not suitable for estimating shade fraction, the  
684 photographic method used in the October field survey is, and it results in an estimate of  
685 2% shade. Given relatively high crop cover during the October sampling period  
686 compared to the others, it is unlikely that the shade cover during the other periods is  
687 much higher than 2%. This is true despite the lower soil zenith angle during the  
688 October sampling period: in April, fields were dominated by low crop residue that do  
689 not cast much shade and in June, low cover from recently germinated crops also do not  
690 cast much shade. This small amount of shade does not seem likely to be able to explain

691 the underestimation of GV and NPV by SMA and MESMA. Thus, a better explanation is  
692 that the endmembers used unmixing for these methods are relatively brighter than  
693 their *in situ* counterparts. And indeed, self-shading of plants (resulting in lower  
694 apparent reflectance than the reflectance of a single leaf) is a common phenomenon.

695 By definition, the normalization procedure must increase fractional cover estimates  
696 (or, do nothing if fractional covers already sum to one). In the case of GV, this  
697 procedure effectively eliminated this bias for GV, lowering RMSE. Normalization  
698 reduced the bias for NPV, thus somewhat lowering RMSE. For soil, normalization  
699 resulted in the opposite bias (i.e., positive MAE), increasing RMSE. Non-normalized  
700 estimates of soil fraction using SMA and MESMA were already low, with very small  
701 biases. Normalization, in effect, overcompensated for this cover component, throwing  
702 off estimates that were already pretty good.

703 Thus, the fact that non-normalized fractions from SMA and MESMA for soil had lower  
704 error than the normalized fractions whereas the opposite is seen with GV and NPV  
705 indicates that neither normalization can be prescribed as a best practice. Not  
706 normalizing, likewise, cannot be prescribed as a best practice. However, the negative  
707 values of  $MAE_c$ , indicating underpredictions in the non-normalized case should be  
708 considered when evaluating SMA and MESMA fractional cover results.

709 Calibration of RSMA to yield absolute cover estimates resulted in cover estimates that  
710 were comparable to those from other methods, as seen in the  $RMSE_c$  (Table 5). The use  
711 of the leave-one-out approach here was necessary so as not to use training data in the  
712 evaluation of error (i.e.  $RMSE_c$ ). But this practice also allows us to examine the variance

713 in the regression coefficients (i.e., slope and intercept). Low variance of the regression  
714 coefficients indicates that, at least in the case examined here, that there is significant  
715 consistency among the various fields in their respective relationships between RSMA  
716 and actual cover. This is likely due to the fact that all fields had similar GV, NPV, and  
717 soil cover during the reference time (April 27; Table 2) and, possibly, that the soil  
718 reflectance of all of the fields is somewhat similar (Figure 2). Further research is needed  
719 to determine the impact of these two factors (similarity of fractional cover during the  
720 reference time and soil spectral characteristics) on RSMA-fractional cover calibrations  
721 at other sites and in other circumstances.

722 The decrease in correlation coefficient between *in situ* fractional cover and calibrated  
723 RSMA compared to uncalibrated RSMA for all ground cover components is intriguing.  
724 All data carry measurement errors, and the estimation of fractional cover of GV, NPV,  
725 and soil in the field is especially difficult, particularly when a binary method is used  
726 (does a brownish green or greenish brown plant count as GV or NPV?). It is possible,  
727 then, that this decrease in correlation coefficient with the addition of field data is due  
728 to error in the *in situ* measurements themselves, or at least variation in the estimated  
729 cover that is endemic to the type of field methods used here. Given our approach, there  
730 is no guarantee that systematic errors in the field data collection would be accounted  
731 for in the regression relationship because the bias/variance on one sampling date may  
732 not be the same as the bias/variance on another sampling date. For instance sampling  
733 bias/variance can be expected to be very different when the vegetation is entirely  
734 green than when it is in between GV and NPV. Even were the human eye able to  
735 determine exactly when a leaf was more green than brown (i.e., spectrally closer to GV

736 than to NPV), the imposition of a binary category (GV vs. NPV) on a fundamentally  
737 continuous property (greenness/brownness) will influence the bias/variance  
738 depending on state of the vegetation. Nonetheless, in practice this error appears to be  
739 not large enough to engender worry, because the  $RMSE_c$  of the calibrated RSMA  
740 fractions are not too different from the  $RMSE_c$  from the other methods and all are  
741 statistically significant when compared with *in situ* data.

742 Nevertheless, if one were only interested in fractional cover of soil, our results suggest  
743 that the calibration of RSMA index values to fractional cover may not be necessary. The  
744 slope near one of the RSMA index values for soil when regressed against *in situ* values  
745 (Table 5) indicates that changes in the RSMA soil index and the actual fractional cover  
746 of soil occur on nearly on a 1:1 basis. The slope near one and intercept near zero of the  
747  $\Delta(\text{RSMA})$  comparison with  $\Delta(f_{GV})$  further supports this conclusion.

748 The results of this study show that the RSMA approach, with the clear tradeoff being  
749 that it cannot – without calibration – be used to estimate absolute cover fractions, has  
750 merit when compared to other remote sensing methods. The fact that RSMA  
751 endmembers were taken from laboratory spectra of green and dry/senescent grass,  
752 rather than from the field area, and that these endmembers allowed RSMA to perform  
753 well compared to methods that required field data underlines the solidity of this  
754 approach; “general” GV and NPV spectra used in the RSMA context resulted in indices  
755 that were strongly correlated with ground component fractional cover and, when these  
756 indices were calibrated, resulted in absolute fractional cover that was as accurate as  
757 MESMA.

758 **Conclusion**

759 Remote sensing of the Earth's terrestrial surface has become a vital tool in the  
760 understanding of the Earth system. The most common use of optical remote sensing  
761 has been in the quantification of GV cover. But GV is not the only component of  
762 terrestrial environments, and for some applications, it is not even the most important  
763 component. This is particularly true in drylands where plants aren't always green and  
764 erosion and/or fire can be a major concern. Other major (non-snow) ground  
765 components, namely NPV and soil, have been increasingly identified as worthy of  
766 study, but a dearth of remote sensing methods that can accurately quantify their  
767 dynamics, in addition to appropriate datasets to calibrate these methods against, has  
768 perhaps hindered scientific advancement in this area.

769 Like all scientific endeavors and perhaps more than most, remote sensing is  
770 characterized by a set of trade-offs. A limited number of photons arriving at a sensor  
771 require tradeoffs between bandwidth, pixel size, and noise. Orbital mechanics constrain  
772 spaceborne platforms requiring tradeoffs between repeat time and swath width. Here,  
773 we observe trade-offs in the amount of data that goes into a technique and how well  
774 that technique can retrieve information about the ground surface; SMA and MESMA  
775 provide better estimates of the changes of GV and NPV than RSMA but at the cost of  
776 needing more ancillary spectral information. We observe tradeoffs in whether  
777 normalization improves or degrades fractional cover estimates; for GV and NPV it  
778 improves estimates, but for soil it does not. We observe tradeoffs in whether SMA or  
779 MESMA, with its greater choice of endmember spectra, improves estimates of fractional  
780 cover; for GV and NPV it does, but for soil it does not. We observe tradeoffs in how

781 addition of information for the calibration of RSMA affects fractional cover estimates; it  
782 reduces the correlation with *in situ* data, but produces results nearly as accurate as  
783 other techniques.

784 These tradeoffs suggest that care must be taken in the choice of methods and our  
785 results indicate that the approach be tailored to purpose of the study. A study aimed at  
786 examining soil cover for the purpose of erosion estimation should utilize a different  
787 method than one aimed at examining NPV cover for fuel load estimation. A study that  
788 needs actual fractional cover should use different methods than one that only needs to  
789 examine changes in fractional cover. Tradeoffs in the methods also suggest that the  
790 method chosen depends, to some extent, on the available data (e.g., endmember  
791 spectra vs. fractional cover of ground components at a specific time).

792 To some extent, but perhaps less than expected, our results indicate the utility of  
793 additional information in the form of added endmembers for the remote sensing of  
794 ground components. One might expect this to be particularly true in the case of soil  
795 due to the amount of variability in soil spectra. However, more information can be too  
796 much of a good thing; one well-chosen soil endmember in SMA provided better soil  
797 cover estimates than a full MESMA approach. RSMA, which requires no soil spectrum,  
798 provided the best quantitative estimates of how soil cover changes. Calibration of  
799 RSMA, which again requires the addition of information, can produce fractional cover  
800 estimates.

801 This study used only nine sites and three dates in an agricultural area with, admittedly,  
802 simple vegetation structure. As a validation exercise, it cannot be said to represent

803 accuracy for all of the chosen models for all vegetation types and locations. Further  
804 study is required for field areas with more complex vegetation structure and more  
805 variable soils. Nonetheless, it is the first study that compares multiple methods for the  
806 estimation of GV, NPV, and soil dynamics and provides guidance on what level of  
807 accuracy might be expected and where biases might exist.

808 But, in addition, this study shows significant differences amongst techniques that have  
809 the same mathematical basis (SMA, RSMA, and MESMA are all spectral unmixing  
810 techniques) and therefore might be thought to produce similar results. Our results  
811 indicate important differences in these techniques showing that, perhaps to an  
812 unexpected degree, the most appropriate technique depends on which ground  
813 component is the focus of study. Our results further suggest diminishing returns with  
814 the inclusion of additional spectral endmembers, an observation that runs counter to  
815 intuition and that can be tested in other locations.

## 816 **Acknowledgments**

817 This research was funded by Australian Research Council Linkage Project Grant  
818 LP0990019 with financial and in-kind contributions from the South Australian  
819 Department for Environment and Natural Resources in Australia and NASA Grants  
820 NNX10AO96G and NNX10AO97G in the US.

821 Thanks to the land-holders, Clinton Tiller and Greg Barr, who graciously gave  
822 permission for collection of cover data from their properties. Thanks to University of  
823 Adelaide staff, Victoria Marshall, Kelly Arbon, Valerie Lawley, Yuot Alaak and Lydia  
824 Cape-Ducluzeau for the many enthusiastic hours of step-point data collection.

825

826 **References**

827 Anderson, E., Bai, Z., Bischof, C., Blackford, S., Demmel, J., Dongarra, J., Du Croz, J.,  
828 Greenbaum, A., Hammarling, S., McKenney, A., & Sorensen, D. (1999). *LAPACK*  
829 *Users' Guide, 3rd Ed.* (3rd ed.). Philadelphia, PA: Society for Industrial and Applied  
830 Mathematics (SIAM)

831 Asner, G.P., & Heidebrecht, K.B. (2002). Spectral unmixing of vegetation, soil and dry  
832 carbon cover in arid regions: comparing multispectral and hyperspectral  
833 observations. *International Journal of Remote Sensing*, 23, 3939-3958

834 Asner, G.P., & Heidebrecht, K.B. (2005). Desertification alters regional ecosystem-  
835 climate interactions. *Global Change Biology*, 11, 182-194

836 Asner, G.P., Wessman, C.A., Bateson, C.A., & Privette, J.L. (2000). Impact of tissue,  
837 canopy, and landscape factors on the hyperspectral reflectance variability of  
838 arid ecosystems. *Remote Sensing Of Environment*, 74, 69-84

839 Ballantine, J.A.C., Okin, G.S., Prentiss, D.E., & Roberts, D.A. (2005). Mapping North African  
840 landforms using continental-scale unmixing of MODIS imagery. *Remote Sensing of*  
841 *Environment*, 97, 470-483

842 Balling, R.C., Jr. (1988). The climatic impact of a Sonoran vegetation discontinuity.  
843 *Climatic Change*, 13, 99-109

844 Ben-Dor, E., & Banin, A. (1994). Visible and near-infrared (0.4-1.1  $\mu\text{m}$ ) analysis of arid  
845 and semiarid soils. *Remote Sensing Of Environment*, 48, 261-274



846 Ben-Dor, E., Goldshleger, N., Benyamini, Y., Agassi, M., & Blumberg, D.G. (2003). The  
847 spectral reflectance properties of soil structural crusts in the 1.2- to 2.5- $\mu$ m  
848 spectral region. *Soil Science Society of America Journal*, 67, 289-299

849 Bonfils, L., de Noblet-Ducoure, N., Braconnot, P., & Joussaume, S. (2001). Hot desert  
850 albedo and climate change: Mid-Holocene monsoon in North Africa. *Journal of*  
851 *Climate*, 14, 3724-3737

852 Chabrillat, S., Goetz, A.F.H., Krosley, L., & Olsen, H.W. (2002). Use of hyperspectral  
853 images in the identification and mapping of expansive clay soils and the role of  
854 spatial resolution. *Remote Sensing Of Environment*, 82, 431-445

855 Chiew, F., Qang, Q.J., McConachy, F., James, R., Wright, W., & deHoedt, G. (2002).  
856 Evaptranspiration Maps for Australia. In, *Hydrology and Water Resources*  
857 *Symposium*. Melbourne, Australia: Institution of Engineers

858 Clark, R.N., King, T.V.V., Klejwa, M., Swayze, G.A., & Vergo, N. (1990). High spectral  
859 resolution reflectance spectroscopy of minerals. *Journal of Geophysical Research*,  
860 95, 12,653-612,680

861 Curran, P.J. (1989). Remote sensing of foliar chemistry. *Remote Sensing Of Environment*, 30,  
862 271-278

863 Dennison, P.E., Halligan, K.Q., & Roberts, D.A. (2004). A comparison of error metrics and  
864 constraints for multiple endmember spectral mixture analysis and spectral  
865 angle mapper. *Remote Sensing Of Environment*, 93, 359-367

866 Elmore, A.J., Asner, G.P., & Hughes, R.F. (2005). Satellite monitoring of vegetation  
867 phenology and fire fuel conditions in Hawaiian drylands. *Earth Interactions*, 9

868 Evans, R.A., & Love, R.M. (1957). The step-point method of sampling: a practical tool in  
869 range research. *Journal of Range Management*, 19, 208-212

870 Franklin, J., Duncan, J., & Turner, D.L. (1993). Reflectance of vegetation and soil in  
871 Chihuahuan desert plant communities from ground radiometry using SPOT  
872 wavebands. *Remote Sensing Of Environment*, 46, 291-304

873 Gerbermann, A.H. (1979). Reflectance of varying mixtures of clay soil and sand.  
874 *Photogrammetric Engineering and Remote Sensing*, 45, 1145-1150

875 Guerschman, J.P., Hill, M.J., Renzullo, L.J., Barrett, D.J., Marks, A.S., & Botha, E.J. (2009).  
876 Estimating fractional cover of photosynthetic vegetation, non-photosynthetic  
877 vegetation and bare soil in the Australian tropical savanna region upscaling the  
878 EO-1 Hyperion and MODIS sensors. *Remote Sensing Of Environment*, 113, 928-945

879 Hapke, B. (1981). Bidirectional reflectance spectroscopy. 1. theory. *Journal of Geophysical*  
880 *Research*, 86, 3039-3054

881 Huete, A., Didan, K., Miura, T., Rodriguez, E.P., Gao, X., & Ferreira, L.G. (2002). Overview  
882 of the radiometric and biophysical performance of the MODIS vegetation  
883 indices. *Remote Sensing Of Environment*, 83, 195-213

884 Jia, G.S.J., Epstein, H.E., & Walker, D.A. (2003). Greening of arctic Alaska, 1981-2001.  
885 *Geophysical Research Letters*, 30, 2067

886 Karnieli, A., Kidron, G.J., Glaesser, C., & Ben-Dor, E. (1999). Spectral characteristics of  
887 cyanobacteria soil crust in semiarid environments. *Remote Sensing Of*  
888 *Environment*, 69, 67-75

889 Kleidon, A., Fraedrich, K., & Heimann, M. (2000). A green planet versus a desert world:  
890 Estimating the maximum effect of vegetation on the land surface climate.  
891 *Climatic Change*, 44, 471-493

892 Lasdon, L.S., & Waren, A.D. (1986). *GRG2 Users Guide*. Cleveland, OH: Cleveland State  
893 University

894 Lobell, D.B., & Asner, G.P. (2002). Moisture effects on soil reflectance. *Soil Science Society*  
895 *of America Journal*, 66, 722-727

896 Lopez, M.V., Gracia, R., & Arrue, J.L. (2000). Effects of reduced tillage on soil surface  
897 properties affecting wind erosion in semiarid fallow lands of Central Aragon.  
898 *European Journal of Agronomy*, 12, 191-199

899 Lucht, W., Prentice, I.C., Myneni, R.B., Sitch, S., Friedlingstein, P., Cramer, W., Bousquet,  
900 P., Buermann, W., & Smith, B. (2002). Climatic control of the high-latitude  
901 vegetation greening trend and Pinatubo effect. *Science*, 296, 1687-1689

902 Mentis, M.T. (1981). Evaluation of the wheel-point and step-point methods of veld  
903 condition assessment. *African Journal of Range and Forage Science*, 16, 89-94

904 Nagler, P.L., Daughtry, C.S.T., & Goward, S.N. (2000). Plant litter and soil reflectance.  
905 *Remote Sensing Of Environment*, 71, 207-215

906 Nagler, P.L., Inoue, Y., Glenn, E.P., Russ, A.L., & Daughtry, C.S.T. (2003). Cellulose  
907 absorption index (CAI) to quantify mixed soil-plant litter scenes. *Remote Sensing*  
908 *Of Environment*, 87, 310-325

909 NASA Land Processes Distributed Active Archive Center (LP DAAC) (2001a). MCD43A4.  
910 In U.E.R.O.a.S.E. Center (Ed.). Sioux City, South Dakota

911 NASA Land Processes Distributed Active Archive Center (LP DAAC) (2001b). MOD13A1.  
912 In U.E.R.O.a.S.E. Center (Ed.). Sioux City, South Dakota

913 Nicholson, S. (2000). Land surface processes and Sahel climate. *Reviews of Geophysics*, 38,  
914 117-139

915 Nidamanuri, R.R., & Zbell, B. (2011). Use of field reflectance data for crop mapping using  
916 airborne hyperspectral image. *Isprs Journal of Photogrammetry and Remote Sensing*,  
917 66, 683-691

918 Okin, G.S. (2007). Relative Spectral Mixture Analysis: a multitemporal index of total  
919 vegetation cover. *Remote Sensing Of Environment*, 106, 467-479

920 Okin, G.S. (2010). The contribution of brown vegetation to vegetation dynamics. *Ecology*,  
921 91, 743-755

922 Okin, G.S., Okin, W.J., Murray, B., & Roberts, D.A. (2001). Practical limits on  
923 hyperspectral vegetation discrimination in arid and semiarid environments.  
924 *Remote Sensing of Environment*, 77, 212-225

925 Okin, G.S., & Painter, T.H. (2004). Effect of grain size on remotely sensed spectral  
926 reflectance of sandy desert surfaces. *Remote Sensing of Environment*, 89, 272-280

927 Palacios-Orueta, A., & Ustin, S.L. (1998). Remote sensing of soil properties in the Santa  
928 Monica Mountains. I. spectral analysis. *Remote Sensing Of Environment*, 65, 170-183

929 Parmesan, C., & Yohe, G. (2003). A globally coherent fingerprint of climate change  
930 impacts across natural systems. *Nature*, 421, 37-42

931 Price, J.C. (1990). On the information content of soil reflectance spectra. *Remote Sensing  
932 Of Environment*, 33, 113-121

933 Reed, B.C. (2006). Trend analysis of time-series phenology of North America derived  
934 from satellite data. *Giscience & Remote Sensing*, 43, 24-38

935 Reed, B.C., Brown, J.F., Vanderzee, D., Loveland, T.R., Merchant, J.W., & Ohlen, D.O.  
936 (1994). Measuring phenological variability from satellite imagery. *Journal of*  
937 *Vegetation Science*, 5, 703-714

938 Roberts, D.A., Gardner, M., Church, R., Ustin, S., Scheer, G., & Green, R.O. (1998).  
939 Mapping chaparral in the Santa Monica Mountains using multiple endmember  
940 spectral mixture models. *Remote Sensing Of Environment*, 65, 267-279

941 Roberts, D.A., Gardner, M., Church, R., Ustin, S.L., & Green, R.O. (1997). Optimum  
942 strategies for mapping vegetation using multiple endmember spectral mixture  
943 models. In, *SPIE Conference Imaging Spectrometry III* (pp. 108-119). San Diego, CA

944 Roberts, D.A., Smith, M.O., & Adams, J.B. (1993). Green vegetation, nonphotosynthetic  
945 vegetation, and soils in AVIRIS data. *Remote Sensing Of Environment*, 44, 255-269

946 Rohlf, F.J., & Sokal, R.R. (1981). *Statistical Tables*. (2 ed.). New York: W.H. Freeman and  
947 Company

948 Schaaf, C.B., Gao, F., Strahler, A.H., Lucht, W., Li, X.W., Tsang, T., Strugnell, N.C., Zhang,  
949 X.Y., Jin, Y.F., Muller, J.P., Lewis, P., Barnsley, M., Hobson, P., Disney, M., Roberts,  
950 G., Dunderdale, M., Doll, C., d'Entremont, R.P., Hu, B.X., Liang, S.L., Privette, J.L.,  
951 & Roy, D. (2002). First operational BRDF, albedo nadir reflectance products from  
952 MODIS. *Remote Sensing Of Environment*, 83, 135-148

953 Shimabukuro, Y.E., & Smith, J.A. (1991). The least-squares mixing models to generate  
954 fraction images derived from remote sensing multispectral data. *IEEE*  
955 *Transactions on Geoscience and Remote Sensing*, N1, 16-20

956 Tucker, C.J. (1979). Red and photographic infrared linear combinations for monitoring  
957 vegetation. *Remote Sensing of Environment*, 8, 127-150

958 Tucker, C.J., Dregne, H.E., & Newcomb, W.W. (1991). Expansion and contraction of the  
959 Sahara Desert from 1980 to 1990. *Science*, 253, 299-301

960 Warren, P.L., & Hutchinson, C.F. (1984). Indicators of rangeland change and their  
961 potential for remote sensing. *Journal of Arid Environments*, 7, 107-126

962 Zhang, X.Y., Friedl, M.A., & Schaaf, C.B. (2006). Global vegetation phenology from  
963 Moderate Resolution Imaging Spectroradiometer (MODIS): Evaluation of global  
964 patterns and comparison with in situ measurements. *Journal of Geophysical  
965 Research-Biogeosciences*, 111

966 Zhang, X.Y., Friedl, M.A., Schaaf, C.B., Strahler, A.H., Hodges, J.C.F., Gao, F., Reed, B.C., &  
967 Huete, A. (2003). Monitoring vegetation phenology using MODIS. *Remote Sensing  
968 Of Environment*, 84, 471-475

969

970

971

972 **Figure Captions**

973 Figure 1. Study site. Fields numbered 1 – 9 were used in this study. The locations where  
974 field spectra were acquired are marked with “X”.

975 Figure 2. Reflectance spectra used as endmembers in RSMA, SMA, and MESMA  
976 unmixing of MODIS NBAR data. The heavy lines are the RSMA endmember spectra  
977 (RSMA does not use a soil endmember), the filled circles are the SMA endmembers, and  
978 the thin lines are the MESMA endmembers. For clarity, only one-half of MESMA soil  
979 endmembers are shown here. SMA and MESMA endmembers are derived from field  
980 spectroscopy.

981 Figure 3. Time series of average values for all fields of *in situ* and remotely-sensed  
982 index/cover values for GV, NPV, and soil. Horizontal bars represent the compositing  
983 time for each remotely-sensed value. End cap symbols depict the ends of vertical bars  
984 representing the standard deviation of index/cover values for all fields on each date.

985 Figure 4. Remotely-sensed index/cover values for GV, NPV, and soil plotted against *in*  
986 *situ* values. Lines are best-fit linear regressions.

987 **Table Captions**

988 Table 1. Field survey dates, MODIS NBAR data composite dates (MODIS production  
989 period), and survey method. All dates are 2010.

990 Table 2. Estimated *in situ* fractional cover.

991 Table 3: Relationship amongst remote sensing indices or estimated cover values of GV  
992 (top quadrant) and for all cover types (pooled, bottom quadrant). Entries with only one  
993 number display the correlations between the indices that do not give absolute  
994 estimates of cover (EVI and RSMA) and other methods. For other entries, the symbol in  
995 parentheses is the sign of the mean absolute difference between the cover values, the  
996 first number is the root mean squared difference (RMSD) between cover values, and the  
997 second number is the correlation ( $r$ ) between cover values. Mean absolute difference  
998 (MAD) is calculated as the cover value for the method in the first column minus the  
999 cover value for the method in the first row.

1000 Table 4: Relationship amongst remote sensing indices or estimated cover values of NPV  
1001 (bottom quadrant) and soil (top quadrant). Entries with only one number display the  
1002 correlations between the indices that do not give absolute estimates of cover (RSMA)  
1003 and other methods. For other entries, the symbol in parentheses is the sign of the mean  
1004 absolute difference between the cover values, the first number is the root mean  
1005 squared difference (RMSD) between cover values, and the second number is the  
1006 correlation ( $r$ ) between cover values. Mean absolute difference (MAD) is calculated as  
1007 the cover value for the method in the first column minus the cover value for the  
1008 method in the first row.

1009 Table 5. Correlation and Regression Analysis of Remote Sensing Results against *in situ*  
1010 Data.

1011 Table 6. Error Metrics of Remote Sensing Fractional Cover Results Compared Against *in*  
1012 *situ* Data.



1013 Table 7: Estimated slope, intercept,  $r$  and RMSE for calibration of RMSA indices using a  
1014 leave-one-out regression approach. Values for slope, intercept, and  $r$  are mean  
1015 (standard deviation). See Equation 8.

Table 1. Field survey dates, MODIS NBAR data composite dates (MODIS production period), and survey method. All dates are 2010.

<b>Field survey</b>	<b>MODIS NBAR Composite Dates (production period)</b>	<b>Survey Method</b>
27-Apr	April 23 – May 8 (2010113)	step-point
22-Jul	July 12 – July 27 (2010193)	step-point
08-Oct	September 30 – October 15 (2010273)	photographic

Table 2. Estimated *in situ* fractional cover.

	Field	$f_{GV}$	$f_{NPV}$	$f_{Soil}$
April 27, 2010	1	0.08	0.60	0.32
	2	0.05	0.63	0.31
	3	0.07	0.65	0.29
	4	0.15	0.52	0.33
	5	0.20	0.50	0.29
	6	0.10	0.65	0.25
	7	0.12	0.58	0.30
	8	0.00	0.66	0.34
	9	0.04	0.70	0.26
July 22, 2010	1	0.16	0.56	0.28
	2	0.40	0.41	0.18
	3	0.27	0.43	0.30
	4	0.16	0.61	0.24
	5	0.34	0.26	0.39
	6	0.39	0.30	0.32
	7	0.23	0.43	0.34
	8	0.39	0.43	0.19
	9	0.23	0.49	0.27
October 8, 2010	1	0.98	0.01	0.01
	2	0.89	0.11	0.00
	3	0.76	0.12	0.12
	4	0.98	0.01	0.01
	5	0.90	0.05	0.04
	6	0.83	0.08	0.09
	7	0.93	0.06	0.01
	8	0.99	0.01	0.00
	9	1.00	0.00	0.00

Table 3: Relationship amongst remote sensing indices or estimated cover values of GV (top quadrant) and for all cover types (pooled, bottom quadrant). Entries with only one number display the correlations between the indices that do not give absolute estimates of cover (EVI and RSMA) and other methods. For other entries, the symbol in parentheses is the sign of the mean absolute difference between the cover values, the first number is the root mean squared difference between cover values, and the second number is the correlation between cover values. Mean absolute difference is calculated as the cover value for the method in the first column minus the cover value for the method in the first row.

	EVI	RSMA	SMA	Norm SMA	MESMA	Norm MESMA
EVI	n/a	0.99	1.00	0.99	1.00	0.99
RSMA	n/a	n/a	1.00	1.00	1.00	1.00
SMA	n/a	n/a	n/a	(-) 0.25, 1.00	(-) 0.01, 1.00	(-) 0.24, 1.00
Norm SMA	n/a	n/a	(+) 0.20, 0.99	n/a	(+) 0.25, 0.99	(+) 0.05, 1.00
MESMA	n/a	n/a	(+) 0.08, 0.91	(-) 0.20, 0.92	n/a	(-) 0.24, 1.00
Norm MESMA	n/a	n/a	(+) 0.23, 0.92	(+) 0.12, 0.93	(+) 0.18, 0.99	n/a

Table 4: Relationship amongst remote sensing indices or estimated cover values of NPV (bottom quadrant) and soil (top quadrant). Entries with only one number display the correlations between the indices that do not give absolute estimates of cover (RSMA) and other methods. For other entries, the symbol in parentheses is the sign of the mean absolute difference between the cover values, the first number is the root mean squared difference between cover values, and the second number is the correlation between cover values. Mean absolute difference is calculated as the cover value for the method in the first column minus the cover value for the method in the first row.

	RSMA	SMA	Norm SMA	MESMA	Norm MESMA
RSMA	n/a	0.92	0.94	0.73	0.73
SMA	0.92	n/a	(-) 0.19, 0.99	(+) 0.08, 0.81	(-) 0.15, 0.80
Norm SMA	0.91	(+) 0.14, 0.99	n/a	(+) 0.22, 0.85	(+) 0.15, 0.85
MESMA	0.92	(+) 0.11, 0.97	(-) 0.06, 0.96	n/a	(-) 0.12, 0.99
Norm MESMA	0.91	(+) 0.28, 0.98	(+) 0.14, 0.98	(+) 0.17, 0.99	n/a

Table 5. Correlation and Regression Analysis of Remote Sensing Results against *in situ* Data.

	GV			NPV			Soil			Pooled		
	<i>r</i>	<i>m</i>	<i>b</i>	<i>r</i>	<i>m</i>	<i>b</i>	<i>r</i>	<i>m</i>	<i>b</i>	<i>r</i>	<i>m</i>	<i>b</i>
EVI	0.99	1.54	-0.13	-	-	-	-	-	-	-	-	-
RSMA	0.99	2.31	0.08	0.89	6.42	0.62	0.92	0.95	-0.64	0.78	1.35	0.33
SMA	0.99	1.50	0.06	0.92	1.97	0.13	0.87	0.86	0.04	0.86	1.36	0.08
Normalized SMA	0.98	0.88	0.05	0.92	1.10	0.12	0.90	0.50	0.03	0.86	0.79	0.07
MESMA	0.99	1.51	0.06	0.93	1.24	0.12	0.84	0.83	0.06	0.94	0.83	0.06
Normalized MESMA	0.99	0.89	0.07	0.93	0.77	0.12	0.84	0.55	0.06	0.93	1.36	0.05
Calibrated RSMA <sup>†</sup>	0.94	0.94	0.03	0.66	0.66	0.08	0.83	0.83	0.03	0.93	0.93	0.03
Δ(EVI)	0.97	1.57	-0.02	-	-	-	-	-	-	-	-	-
Δ(RSMA)	0.96	2.35	-0.02	0.68	6.43	0.02	0.84	0.99	0.02	0.85	1.91	0.00
Δ(SMA)	0.96	1.50	-0.01	0.77	2.15	0.07	0.63	0.62	-0.04	0.94	1.42	0.01
Δ(Normalized SMA)	0.94	0.91	-0.05	0.79	1.16	0.04	0.74	0.40	-0.04	0.94	0.83	0.00
Δ(MESMA)	0.96	1.50	0.01	0.85	1.43	0.10	0.80	0.67	-0.11	0.95	1.31	0.02
Δ(Normalized MESMA)	0.96	0.87	0.01	0.81	0.78	0.02	0.83	0.46	-0.11	0.96	0.81	0.00

<sup>†</sup> *r*, *m*, and *b* calculated here with omitted data from leave-one-out procedure.

Table 6. Error Metrics of Remote Sensing Fractional Cover Results Compared Against *in situ* Data.

	GV		NPV		Soil		Pooled	
	MAE <sub>c</sub>	RMSE <sub>c</sub>	MAE <sub>c</sub>	RMSE <sub>c</sub>	MAE <sub>c</sub>	RMSE <sub>c</sub>	MAE <sub>c</sub>	RMSE <sub>c</sub>
EVI	-	-	-	-	-	-	-	-
RSMA	-	-	-	-	-	-	-	-
SMA	-0.19	0.23	-0.24	0.29	-0.02	0.07	-0.15	0.21
Normalized SMA	0.00	0.08	-0.14	0.17	0.14	0.19	0.00	0.16
MESMA	-0.19	0.23	-0.16	0.19	-0.03	0.08	-0.13	0.11
Normalized MESMA	-0.02	0.07	-0.04	0.12	0.06	0.13	0.00	0.18
Calibrated RSMA <sup>†</sup>	0.00	0.10	0.00	0.18	0.00	0.09	0.00	0.13
Δ(EVI)	-	-	-	-	-	-	-	-
Δ(RSMA)	-	-	-	-	-	-	-	-
Δ(SMA)	-0.17	0.22	0.16	0.23	-0.02	0.13	-0.01	0.20
Δ(Normalized SMA)	0.10	0.15	0.02	0.14	-0.12	0.22	0.00	0.17
Δ(MESMA)	-0.17	0.22	0.04	0.13	0.09	0.14	-0.01	0.17
Δ(Normalized MESMA)	0.06	0.12	-0.13	0.19	0.07	0.18	0.00	0.17

<sup>†</sup> *r*, *m*, and *b* calculated here with omitted data from leave-one-out procedure.

Table 7: Estimated slope, intercept,  $r$  and RMSE for calibration of RMSA indices using a leave-one-out regression approach. Values for slope, intercept, and  $r$  are mean (standard deviation). See Equation 8.

	GV	NPV	Soil
Slope	2.35 (0.04)	6.44 (0.50)	0.99 (0.04)
Intercept	-0.02 (0.01)	0.02 (0.03)	-0.97 (0.03)
$r$	0.96 (0.00)	0.68 (0.04)	0.84 (0.01)
MAE	-0.00084	-0.0045	0.00066
RMSE	0.10	0.18	0.09

Figure 1  
[Click here to download high resolution image](#)

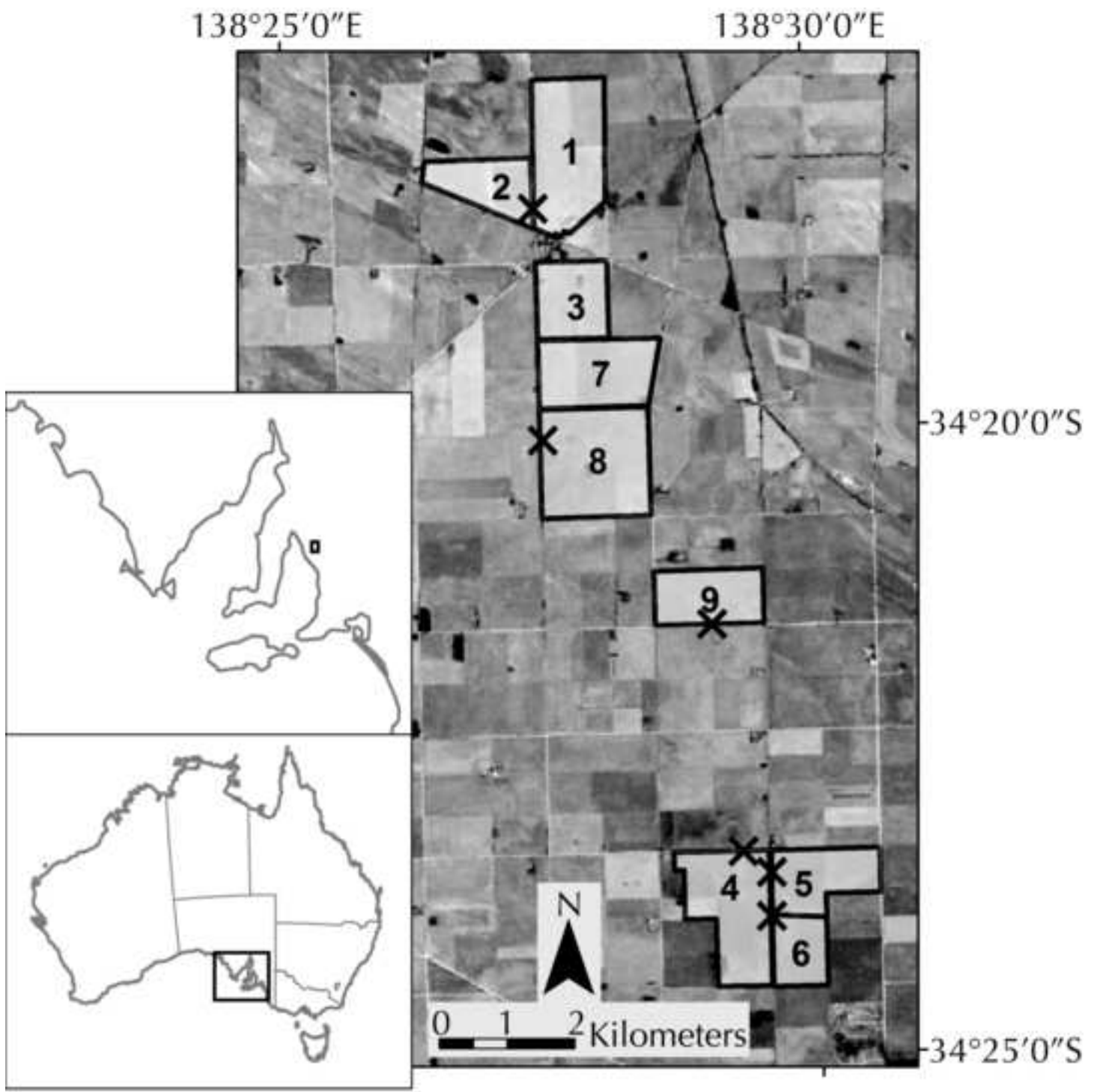


FIGURE 1

Figure 2

[Click here to download high resolution image](#)

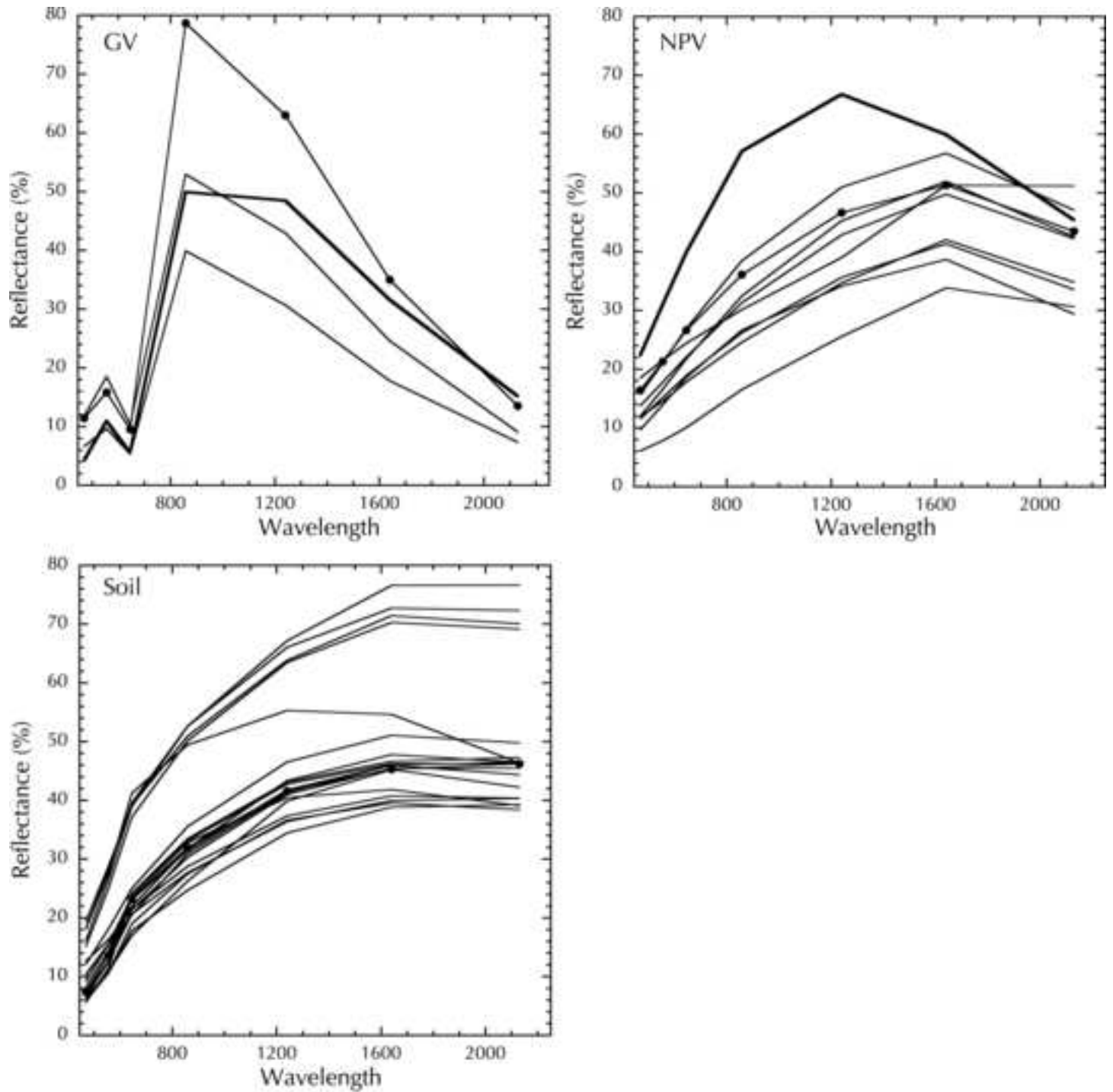


FIGURE 2



Figure 3  
[Click here to download high resolution image](#)

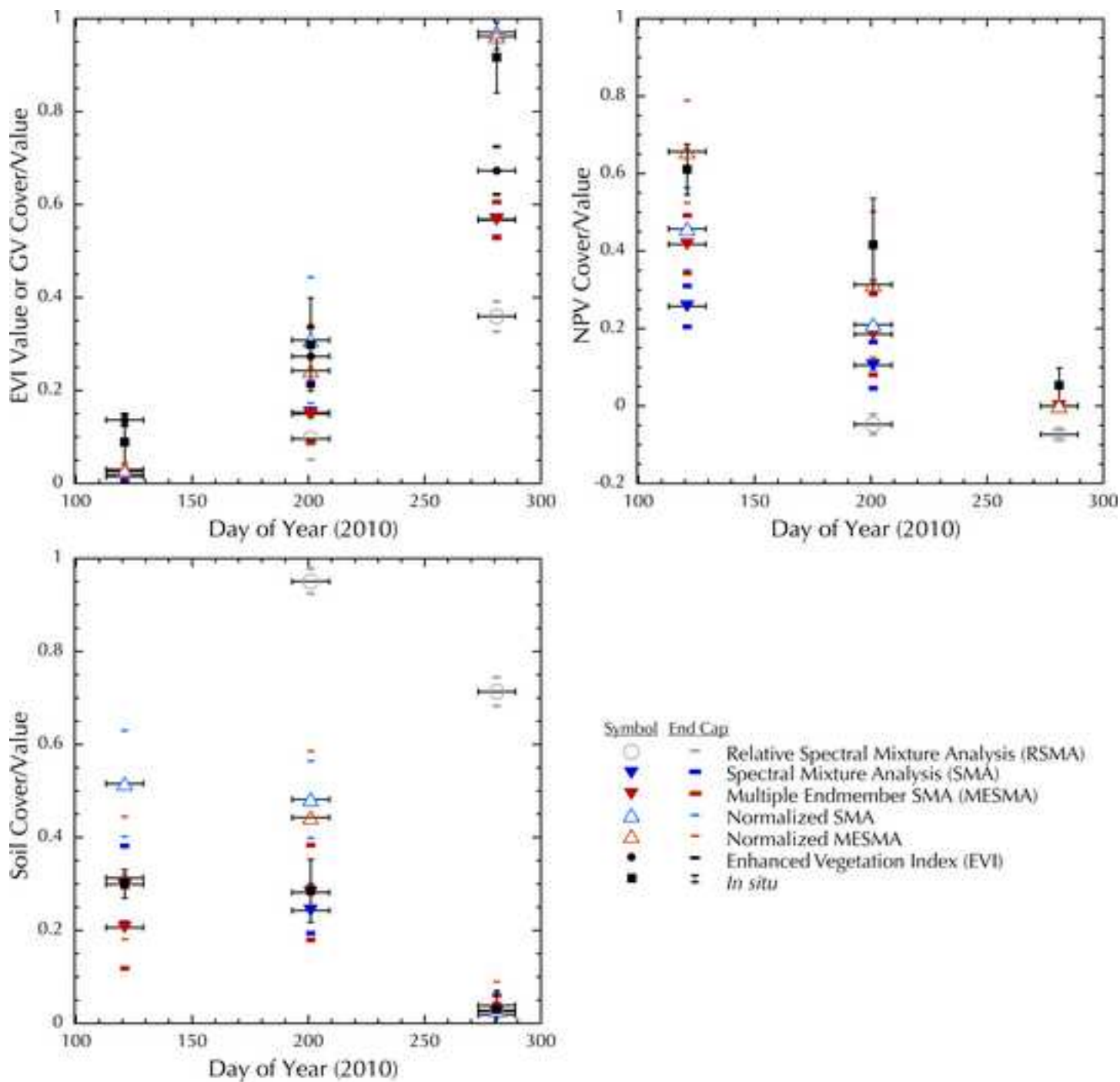


FIGURE 3

Figure 4

[Click here to download high resolution image](#)

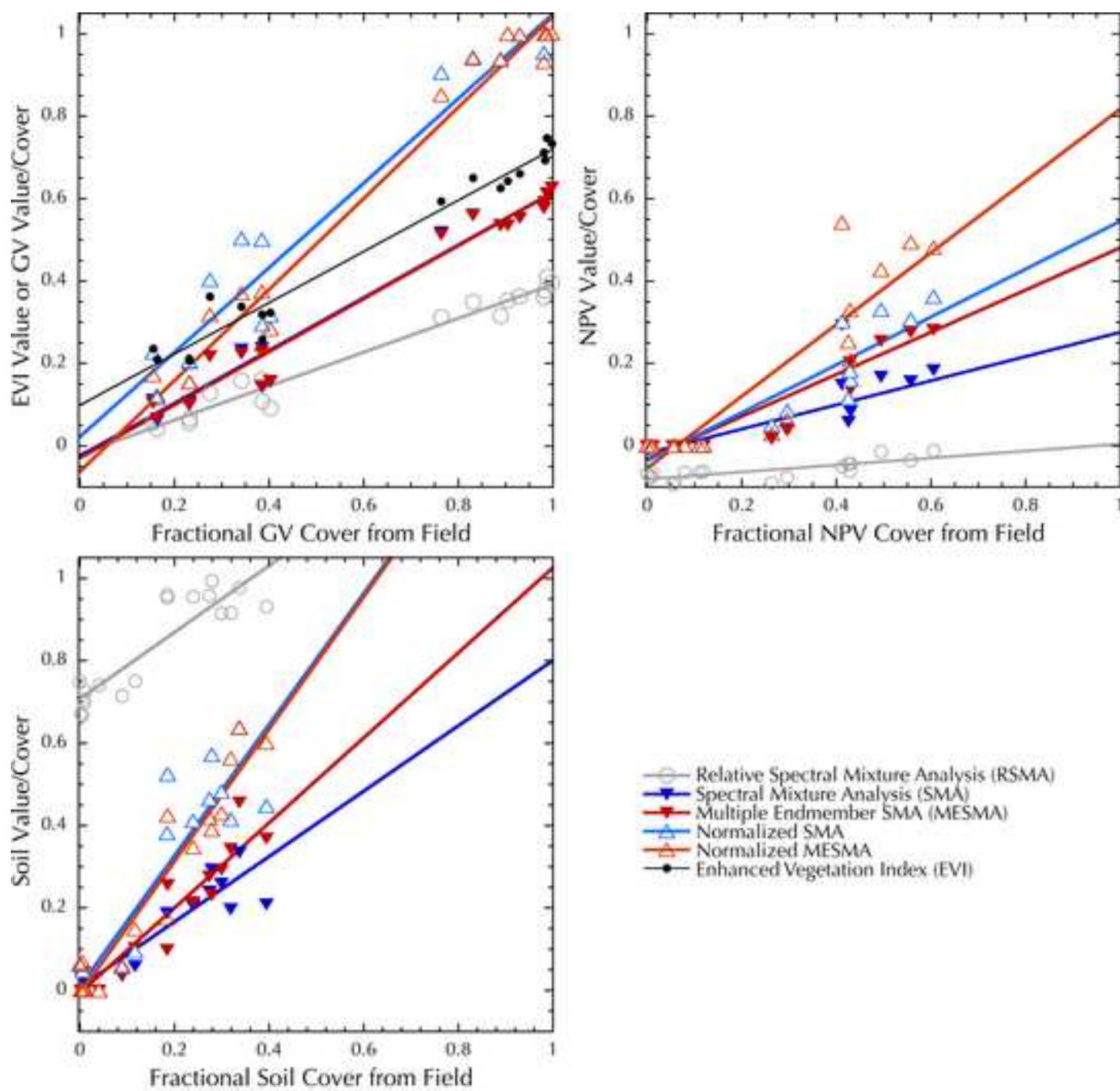


FIGURE 4